INFN Istituto Nazionale di Fisica Nucleare
Laboratori Nazionali di Frascati

SPARC

SPARC-GE-03/002
11 May 2003

CONTRIBUTIONS TO PAC 2003

(11-17 May 2003, Portland, Oregon, USA)

- The sparc project: a high brightness electron beam source at LNF to drive a SASE-FEL experiment

- Beam dynamics studies for the SPARC project

- Start to end simulations for the SPARX proposal

- Study and design of room temperature cavities for a rf compressor prototype

- Self-consistent 3D PIC code for modeling of high-brightness beams

- Code comparison for simulations of photo-injectors

- Study of a low impedance beam position monitor for short bunches

- Design and status of the VISA II experiment

THE SPARC PROJECT: A HIGH BRIGHTNESS ELECTRON BEAM SOURCE AT LNF TO DRIVE A SASE-FEL EXPERIMENT

D.Alesini, S.Bertolucci, M.E.Biagini, C.Biscari, R.Boni, M.Boscolo, M.Castellano, A.Clozza, G.Di Pirro, A.Drago, A.Esposito, M.Ferrario, V.Fusco, A.Gallo, A.Ghigo, S.Guiducci, M.Incurvati, C.Ligi, F.Marcellini, M.Migliorati, C.Milardi, L.Palumbo, L.Pellegrino, M.Preger, P.Raimondi, R.Ricci, C.Sanelli, M.Serio, F.Sgamma, B.Spataro, A.Stecchi, A.Stella, F.Tazzioli, C.Vaccarezza, M.Vescovi, C.Vicario, M.Zobov, *INFN-Frascati*

F.Alessandria, A.Bacci, I.Boscolo, F.Broggi, S.Cialdi, C.DeMartinis, D.Giove, C.Maroli, V.Petrillo, M.Romè, L.Serafini, *INFN-Milano*

D.Levi, M.Mattioli, G.Medici, *INFN-Roma1*

L.Catani, E.Chiadroni, S.Tazzari, *INFN-Roma2*

R.Bartolini, F.Ciocci, G.Dattoli, A.Doria, F.Flora, G.P.Gallerano, L.Giannessi, E.Giovenale, G.Messina, L.Mezi, P.L.Ottaviani, L.Picardi, M.Quattromini, A.Renieri, C.Ronsivalle, *ENEA-Frascati*

A.Cianchi, A.D'Angelo, R.Di Salvo, A.Fantini, D.Moricciani, C.Schaerf, *Università Roma Tor Vergata*

J.B. Rosenzweig, *UCLA - Dept. of Physics and Astronomy*

Abstract

The Project SPARC (Sorgente Pulsata e Amplificata di Radiazione Coerente), proposed by a collaboration among ENEA-INFN-CNR-Universita` di Roma Tor Vergata-INFM-ST, was recently funded by the Italian Government. The aim of the project is to promote an R&D activity oriented to the development of a coherent ultra-brilliant X-ray source in Italy (SPARX proposal [1]). The SPARC collaboration identified a program based on two main issues: the generation of ultra-high peak brightness electron beams and experimental study of SASE-FEL process with generation of resonant higher harmonics. The SPARC project is being designed in order to encompass the construction of an advanced photo-injector producing a 150-200 MeV beam to drive a SASE-FEL in the optical range. The machine will be built at LNF, inside an underground bunker: it is comprised of an rf gun driven by a Ti:Sa laser, injecting into three SLAC accelerating sections. We foresee conducting investigations on the emittance correction[2] and on the rf compression techniques[3], which are expected to increase the peak current achievable at the injector exit up to kA level, with proper preservation of the transverse emittance. Although the system is expected to drive a FEL experiment, it can be used also to investigate beam physics issues like surface-roughness-induced wake fields, bunch-length measurements in the sub-ps range, emittance degradation in magnetic compressors due to CSR, and Compton backscattering production of sub-ps X-ray pulses.

PROJECT OVERVIEW

The overall SPARC Project consists of 4 main lines of activity:

1) *150 MeV Advanced Photo-Injector*: the performances of X-ray SASE-FEL's are critically dependent on the peak brightness of the electron beam delivered at the undulator entrance. Two main issues to investigate: generation of the electron beam and compression via magnetic and/or velocity bunching.
2) *SASE-FEL Visible-VUV Experiment*: this is aimed to investigate the problems related to the beam matching into an undulator and the alignment with the radiation beam, as well as the generation of non-linear coherent higher harmonics. The SASE FEL experiment will be performed with the 150 MeV beam, using a segmented undulator with additional strong focusing to observe FEL radiation at 500 nm and below.
3) *X-ray Optics/Monochromators*: the X-ray FEL radiation will provide unique radiation beams in terms of peak brightness and pulse time duration (100 fs). This project will pursue a vigorous R&D activity on the analysis of radiation-matter interactions in the spectral range of SASE X-ray FEL's (from 0.1 to 10 nm), and on the design of new optics and monochromators.
4) *Soft X-ray table-top Source:* to test these optics and start the R&D on applications the project will undertake the upgrade of the presently operated table-top source of X-rays at INFM - Politecnico Milano, delivering 10^7 soft X-ray photons in 10-20 fs pulses by means of high harmonic generation in a gas.

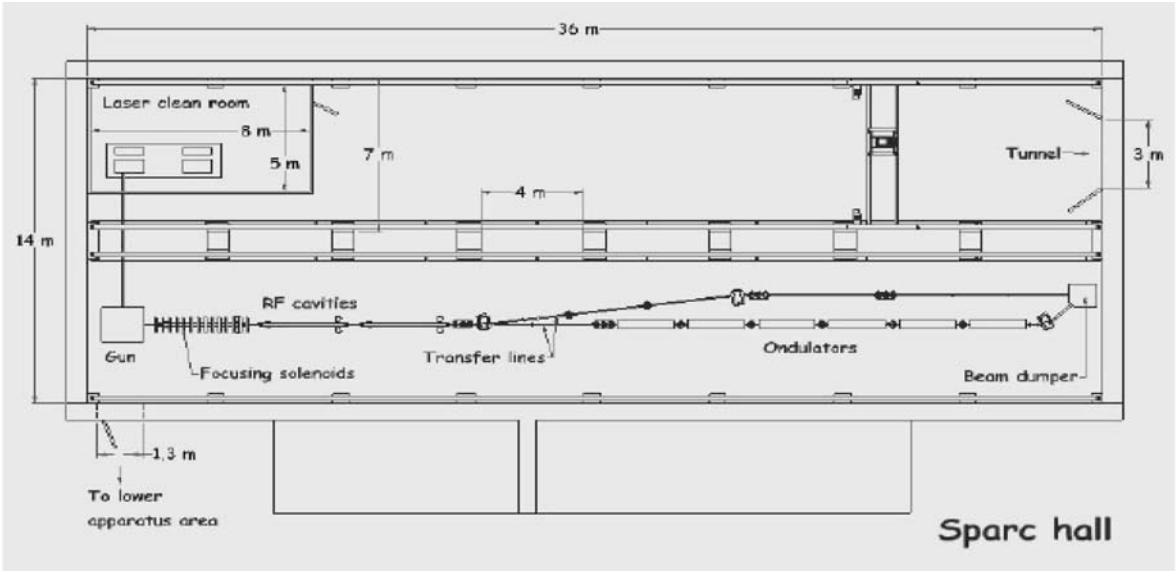

Figure 1 : Lay-out of SPARC Advanced Photo-Injector and SASE-FEL Experiment

In the following we present an overview of the design for the system under construction at the Frascati National Laboratories of INFN, by a collaboration between two national research institutions, INFN and ENEA namely, aiming at reaching the scientific and technological goals indicated in the first two topics listed above, *i.e.* the production of a high brightness electron beam and the operation at saturation of a SASE-FEL experiment driven by such an electron beam.

ADVANCED PHOTO-INJECTOR

The main goals of this activity are the acquisition of expertise in the construction, commissioning and characterization of an advanced photo-injector system and the experimental investigation of two new ideas that have been recently conceived and presented by the study group: the optimum working point for high brightness RF photo-injectors and RF bunch compression technique.

The 150 MeV injector will be built inside an available bunker of the Frascati INFN National Laboratories: the general layout of the system is shown in Fig. 1. The system consists of a 1.6 cell RF gun operated at S-band (2.856 GHz, of the BNL/UCLA/SLAC type) and high peak field on the cathode (120 MeV/m) with incorporated metallic photo-cathode (Cu or Mg), generating a 6 MeV beam[4]. The beam is then focused and matched into 3 accelerating sections of the SLAC type (S-band TW) which accelerates the bunch up to 150-200 MeV. For the Laser system it is planned to use the third harmonic of the radiation from a Ti:Sa laser with the oscillator pulse train locked to the RF . To obtain the time pulse shape we are going to test the manipulation of frequency lines in the large bandwidth of Ti:Sa, in order to produce the 10 ps flat top shape. We can use a liquid crystal mask in the Fourier plane for nondispersive optic arrangement or a collinear acusto-optic modulator for line frequency manipulation. The goal of these tests is to obtain a pulse rise time shorter than 1 ps with intensity ripples along the 10 ps pulse smaller than 30% (peak to peak): under such a condition the beam emittance achievable at the end of the photo-injector is foreseen to be smaller than 1 μm.

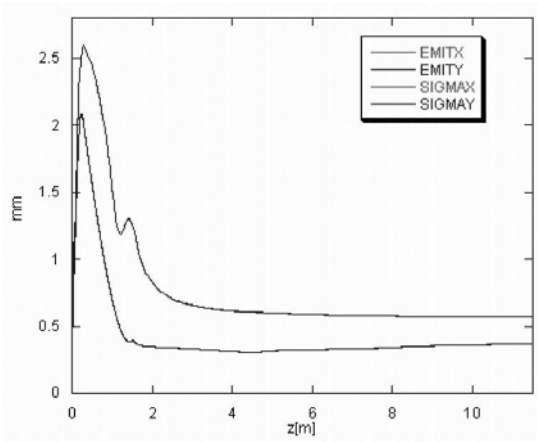

Figure 2: Parmela simulation of emittance and envelope evolution along the SPARC photo-injector (only two accelerating sections taken into account)

The first experiment is planned to verify the beam emittance compensation process. The key point is the measurement, at different bunch charges, of the emittance oscillation in the drift after the gun where a double minima behavior is expected. The optimum beam matching to the booster is predicted on the relative maximum, see Fig. 2. A dedicated movable emittance measurement station has been designed, as shown in Fig. 3. Our simulations using PARMELA indicate that we can generate in this way a beam as required by the FEL experiment at 150 MeV. The rms correlated energy

spread is 0.2% with a rms norm. emittance lower than 2 μm (at 1 nC bunch charge, 85 peak current). The slice energy spread and the slice norm. emittance, calculated over a 300 μm slice length, are below 0.05% and 1 μm respectively, all over the bunch. A complete investigation over the parameter range of the system is in progress, in particular tolerances and sensitivities are being considered in the beam dynamics simulations [5].

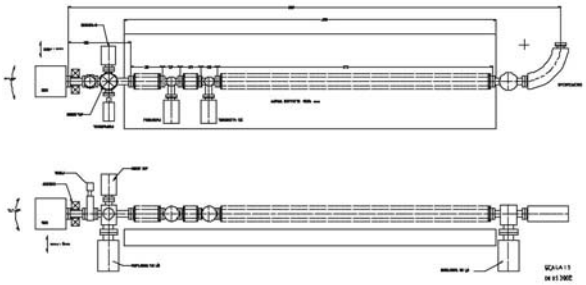

Figure 3: movable emittance measurement station. A pepperpot and a screen are connected with three bellows in order to scan the emittance along 1m long drift

SASE FEL EXPERIMENT

The FEL SASE experiment will be conducted using a permanent magnet undulator made of 6 sections, each 2.13 m long, separated by 0.36 m gaps hosting single quadrupoles which focus in the horizontal plane. The undulator period is set at 3.0 cm, with an undulator parameter k_w = 1.4. A simulation performed with GENESIS is reported in Fig. 4, showing the exponential growth of the radiation power along the undulator. Almost 108 Watts can be reached after 14 m of total undulator length. Preliminary evaluations of the radiation power generated into the non-linear coherent odd higher harmonics show that 10^7 and $7x10^5$ W can be reached on the third and fifth harmonics, respectively.

FURTHER EXPERIMENTS

Two main upgrades will be implemented in a second phase of the project. A dedicated accelerating section will be inserted downstream the RF gun in order to exploit the full potentialities of the velocity bunching technique. Furthermore, in the parallel beam line a magnetic chicane will be installed to allow the experimental investigation of CSR induced effects on emittance degradation and surface roughness wake-field effects. Its design and construction will proceed in parallel to the commissioning of the SPARC injector system (RF gun + 3 standard SLAC-type 3 m sections). These tests are of great relevance in our R&D program in view of the development of a coherent X-ray source according to the SPARX proposal[1], the general layout of which foresees a mixed compression scheme: RF compression in the photo-injector and one single stage magnetic compression at 1 GeV up to the final peak current of 2.5 kA.

Applying velocity bunching in the SPARC photo-injector with low charge bunches (about 15 pC) will allow the production of ultra-short electron bunches, in the range of a few μm rms bunch length, fully synchronized to the Ti:Sa laser pulses. A further upgrade of the laser system to produce multi-TW pulses, by means of a third stage of amplification and an under vacuum pulse compressor, will allow to conduct laser wake-field plasma acceleration experiments with external injection of high quality ultra-short bunches into the plasma wave, for ultra-high gradient acceleration of electron beams.

This naturally projects SPARC as a more general test facility to conduct advanced beam physics and new acceleration technique experiments at LNF in the near future.

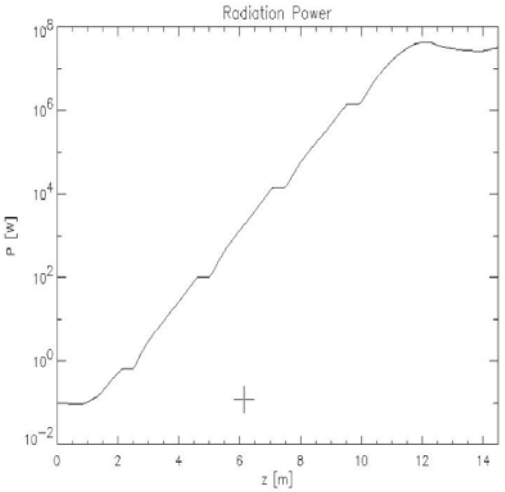

Figure 4: FEL radiation power growth along the undulator

REFERENCES

[1] D. Alesini *et al*., *Conceptual design of a High Brightness Linac for Soft X-Ray SASE-FEL Source* , Proceedings of the FEL-2002 Int. Conference

[2] M. Ferrario *et al*., *Recent Advances and Novel Ideas for High Brightness Electron Beam Production based on Photo-Injectors*, INFN Rep. LNF-03/06 (P), May 2003

[3] L. Serafini and M. Ferrario, *Velocity Bunching in Photo-Injecto*rs, *AIP CP* **581** (2001) 87

[4] D.T. Palmer, PhD. Thesis, Stanford University

[5] M. Biagini *et al*., *Beam Dynamics Studies for the SPARC Project,* this conference

BEAM DYNAMICS STUDIES FOR THE SPARC PROJECT

M. Biagini, M. Boscolo, M. Ferrario, V. Fusco, S. Guiducci, M. Migliorati, Vaccarezza,
INFN-LNF, Frascati, ITALY
L. Serafini, INFN-Mi, Milan, ITALY
R. Bartolini, L. Giannessi, M. Quattromini, C. Ronsivalle, ENEA-Frascati, ITALY
C. Limborg, SLAC, Stanford, USA, J. B. Rosenzweig, UCLA, Los Angeles, USA

Abstract

The aim of the SPARC project, is to promote an R&D activity oriented to the development of a high brightness photoinjector to drive SASE-FEL experiments. We discuss in this paper the status of the beam dynamics simulation activities.

INTRODUCTION

The SPARC photoinjector has to drive a SASE FEL experiment at 530 nm [1]. To meet the FEL requirements a high brightness electron beam has to be generated, accelerated up to 155 MeV and transported up to the entrance of the undulator, minimizing the emittance and energy spread degradation due to correlated space charge and wake field effects. In order to saturate the FEL radiation in the planned 15 m long undulator, and to additionally allow generation of higher harmonics, the design beam parameters are very rigorous: normalized emittance ε_n < 1 μm, relative energy spread $\Delta\gamma/\gamma$ < 0.1 % and peak current I ~ 90 A. Fortunately, such parameters have to be reached only on the scale of the FEL cooperation length, which in our case is less than 300 μm.

START TO END SIMULATIONS

The accelerator consists of a 1.6 cell RF gun operated at S-band with a peak field on the cathode of 120 MV/m and an incorporated metallic photo-cathode followed by an emittance compensating solenoid and three accelerating sections of the SLAC type (S-band, travelling wave). A transfer line made with two triplets allows the matching with the undulator optics (see Fig. 1). A start-to-end simulation of the beam dynamics from the injector through transfer line and undulator system has been performed by means of the codes PARMELA [2] and GENESIS [3].

We take as our example the most conservative system that is to be encountered, one with no velocity bunching [1], and a relatively low energy of 155 MeV (consistent with either low gradient, three TW section operation, or high gradient, two TW section operation). The temporal profile of the bunch has been taken uniform over 11.5 ps with a rising time of 1 ps, a laser spot on the cathode of 1 mm and a 1 nC charge, with a 35 degree launch phase in the gun, 0.27 T of solenoid field and on-crest acceleration in the linac. We decided to place a set of coils around the first accelerating structure (700 G), to provide additional flexibility in the choice of the accelerating gradient (25 MV/m in the simulations).

The transverse emittance compensation process is visible in figure 2: the emittance reaches an absolute maximum in the centre of the solenoid and it is reduced to a minimum in the drifting section, then begins again to increase. The booster entrance is located at the envelope laminar waist corresponding to an emittance relative maximum [4]. The emittance oscillation is driven by a properly matched accelerating field [5] down to an absolute minimum (~0.6 μm) at the linac exit where the average bunch energy is 155 MeV, high enough to damp space charge forces. The estimated thermal emittance (0.3 μm), included in the simulation, results to be in the present design the main contribution to the total emittance.

As expected, the emittance along the transfer line and in the undulator is not anymore affected by space charge effects even when the beam has to be focused to a very small spot (~55 μm) to meet the undulator matching conditions.

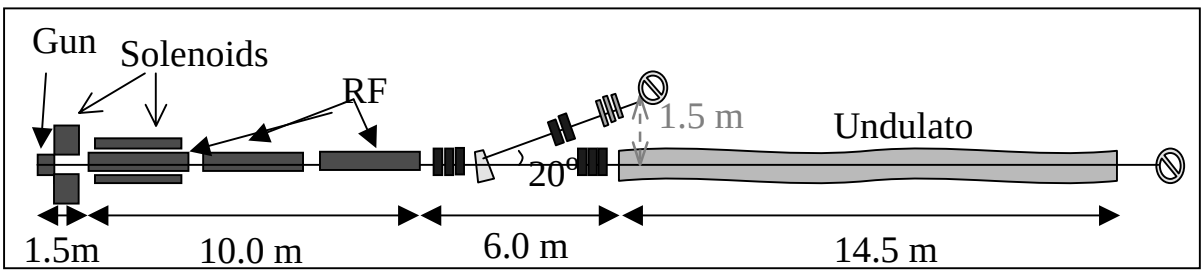

Figure 1: Schematic layout of SPARC phase 1

Transverse and longitudinal phase spaces at the entrance of the undulator are shown in figure 3. Despite some halo observed in the transverse phase space related to the bunch tails mismatch, the core of

the bunch is very good behaved, having a 0.6 μm rms normalized emittance in both planes.

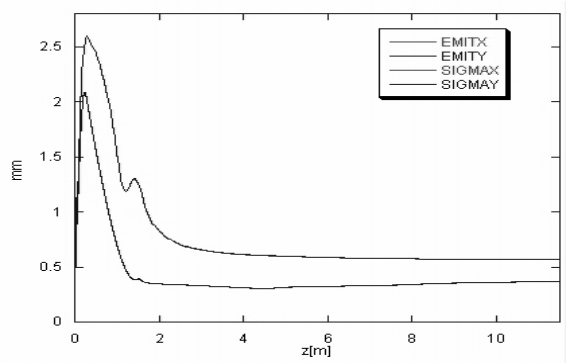

Figure 2: PARMELA simulation of the rms normalized emittance and bunch envelope evolution along the SPARC injector up to 11.5 m.

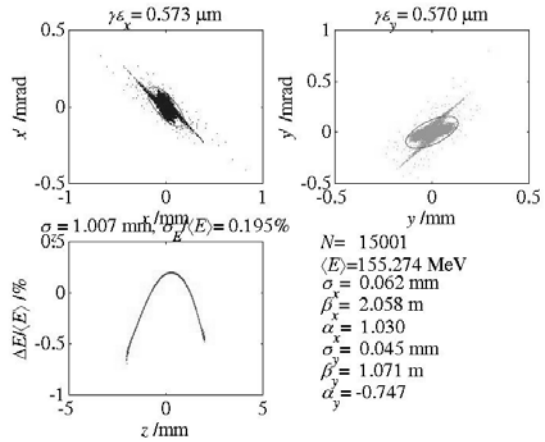

Figure 3: Transverse and longitudinal phase spaces at the entrance of the undulator.

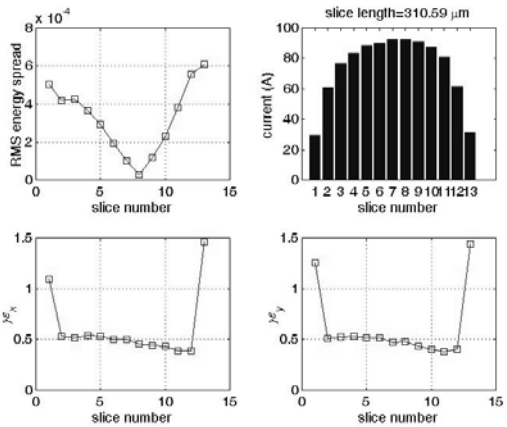

Figure 4: Slice analysis of beam properties at the undulator entrance.

The longitudinal phase space shows the typical energy phase correlation induced mainly by the RF field, with little contribution from longitudinal space-charge, having relative rms energy spread lower than 0.2% as required. The slice analysis performed at the undulator entrance is shown in figure 4. Slice emittance and energy spread are well below the nominal design values for more than 85% of the bunch length. The slice peak current is above 60 A in the same region.

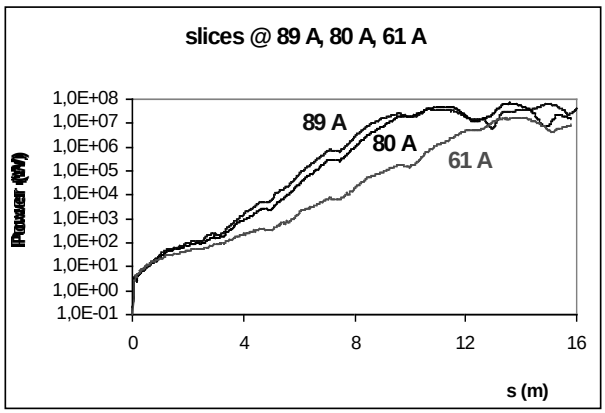

Figure 5: GENESIS simulations of the FEL for three representative slices along the bunch.

The analysis of the FEL performance has been performed with the code GENESIS, taking in to account three representative slices along the bunch provided by PARMELA, showing that even the radiation emitted by the slices closer to the tails that contain a lower local value of the current (61 A) can reach saturation as shown in figure 5.

SENSITIVITY STUDIES

Once the nominal parameters are set we have to provide also stable operation and tolerate some jitter in the nominal value of the parameters . In this section we discuss only two selected topics of such studies performed thus far, in which cathode emission uniformity, laser beam ellipticity, laser centroid offset, laser time structure, and solenoid field errors have been explored.

The effects of cathode's dishomogeneities [6] have been tested by simulating, using the code TREDI [7], a zone on the cathode with reduced quantum efficiency QE. We have assumed a circular QE "hole" with a surface 10% of the nominal bunch spot, centered half-way of the bunch radius. The results suggest that localized inhomogeneities do not dramatically degrade the emittance, growing by $\Delta\varepsilon_{x(y)} \approx 10\%\,(15\%)$ for QE $\approx$ 70% as reported in figure 6. This analysis will be further extended to the cases of randomly distributed ("spotty") inhomogeneities, which better describe the behavior of real cathodes.

Flat top laser pulses with rise times shorter than1 ps are required in order to avoid emittance degradation [8], as shown in figure 7.

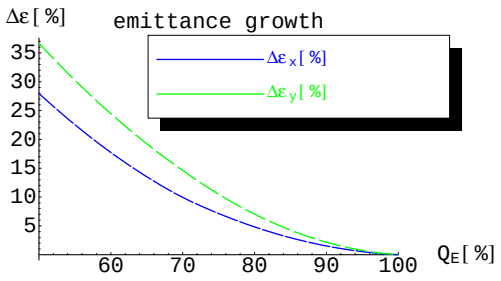

Figure 6: **:** Emittance growth as a function of Q_E .

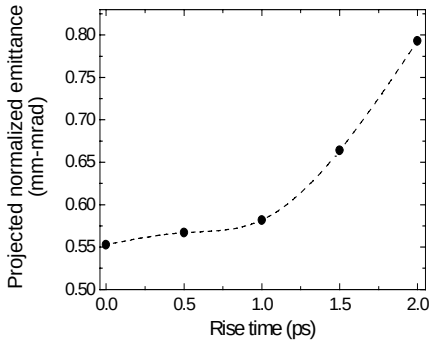

Figure 7: **:** Norm. rms emittance versus rise time.

But laser pulse shaping with short rise time may result in the formation of longitudinal ripples. Therefore, the effect of a laser pulse with longitudinal ripples has been investigated. The beam is assumed to be transversely uniform in these studies. The striking result is that even with a 30% of longitudinal irregularity the beam emittance degradation is limited to 6%. This result can be interpreted as if the space-charge force induces a compensation of the longitudinal irregularity. This hypothesis is justifed by PARMELA simulation results. In figure 8 the evolution of longitudinal beam distributions are displayed. At the cathode the temporal spectrum has a 30 % ripple overlapped on a square pulse, the relative energy spread is zero. As the beam goes through the gun and drifts the temporal oscillations transform in energy oscillations. At the entrance of the first acceleration structure (at z=150 cm) the beam has lost the temporal ripples, which have converted into energy variations through a fractional plasma oscillation. These energy ripples do not have any notable effect to the rms energy spread at the end of the linac, as they are soon suppressed inside the first accelerating structure. These results indicate that the shape of the laser pulse should be square with a very small rise time, whether a smooth temporal profile is not a stringent requirement.

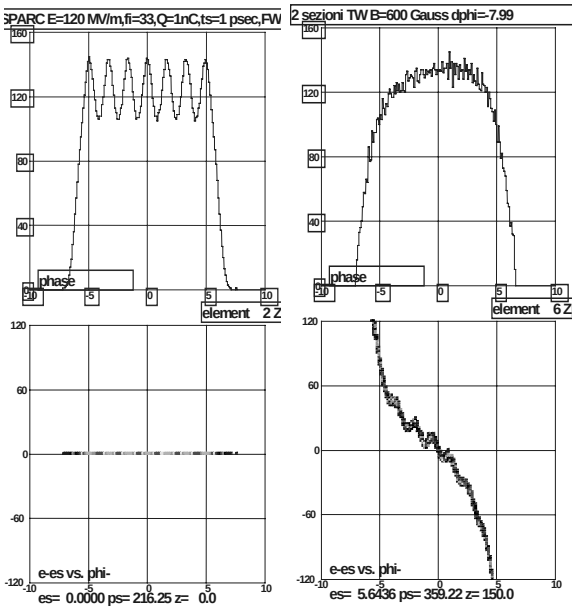

Figure 8: : Longitudinal beam distribution: phase and energy spectrum in the upper and lower plots, respectively. Left plot: initial distribution at cathode (z=0 m); right plot: beam at z=1.5 m.

CONCLUSIONS

Start to end simulation of the optimal SPARC working point have shown that we can meet the FEL requirements with a reasonable parameter set. The requirements on the longitudinal and transverse profile of the laser pulse, the phase jitters, the laser pointing stability have been set. Preliminary sensitivity studies have not shown dramatic concerns about the possibility of stable operation. A more systematic [9] study is in progress .

REFERENCES

[1] L. Palumbo et al., "The SPARC Project: A High-Brightness Electron Beam Source to Drive a SASE-FEL Experiment at LNF", this conference.
[2] J. Billen, "PARMELA", LA-|UR-96-1835, 1996.
[3] S. Reiche, Nucl. Instrum. & Meth. A429,243 (1999).
[4] M.Ferrario et al., "HOMDYN Studies for the LCLS RF Photoinjector", Proc. of ICFA Workshop on the Physics of High Brightness Beams, UCLA, Nov. 1999
[5] L.Serafini,J.Rosenzweig,*Phys. Rev. E* **55**(1997) 7565
[6] F. Zhou et al.,PRST-AB, V. 5, 094203 (2002).
[7] L. Giannessi, M. Quattromini, Submitted to PRST AB (2003).
[8] J. Yang, J. of Appl. Phys., V. 92, N. 1, (2002)
[9] C. Limborg, "New optimization for the LCLS photo-injector", Proc. Of EPAC-02, Paris 2002.

START TO END SIMULATIONS FOR THE SPARX PROPOSAL

M. Biagini, M. Boscolo, M. Ferrario, V. Fusco, S. Guiducci, B. Spataro, C. Vaccarezza, M. Zobov
INFN-LNF, Frascati, ITALY
L. Serafini, INFN-Mi, Milan, ITALY
R. Bartolini, G. Dattoli, L. Giannessi, L. Mezi, M. Quattromini, C. Ronsivalle,
ENEA-Frascati, ITALY
E. Chiadroni, University of Rome II, Rome, ITALY
P. Emma, SLAC, Stanford, USA
J. B. Rosenzweig, UCLA, Los Angeles, USA

Abstract

We report in this paper the results of start to end simulations concerning the SPARX option based on an S-band normal conducting linac. One of the most critical systems is the bunch compressor. The effects on beam dynamics of a magnetic chicane system and a rectilinear RF compressor integrated in a high brightness photoinjector, are analyzed and compared in this paper.

INTRODUCTION

The SPARX proposal is devoted to the realization in Italy of a large scale ultra-brilliant and coherent X-ray source [1]. Two spectral complementary regions around 13.5 nm and 1.5 nm, are considered for the radiation source. A preliminary set of the required beam parameters are reported in table 1. Two basic schemes have been considered for the Linac, as shown in figure 1: the first one, the Hybrid Scheme, consists in an advanced high brightness photoinjector, with a RF compression stage [2], followed by a first linac (Linac 1) that drives the beam up to 0.5 GeV with the correlated energy spread required to compress the beam in the next magnetic chicane. The second linac (Linac 2) drives the beam up to 2.5 GeV while damping the correlated energy spread, taking profit of the effective contribution of the longitudinal wake fields provided by the S-band accelerating structures.

Table 1 – Beam Parameters

Beam Energy	2.5	GeV
Peak current	2	KA
Emittance (projected)	2	μm
Emittance (slice)	1	μm
Energy spread	0.1	%

In the Fully Magnetic Scheme the first compression stage is provided by a magnetic chicane after the Linac 1 at 350 MeV. An intermediate linac section, Linac 2, drives the beam up to 1 GeV. The next magnetic chicane compresses the beam up to the project requirements. The final Linac 3 brings the beam up to 2.5 GeV, while compensating the final energy spread of the beam.

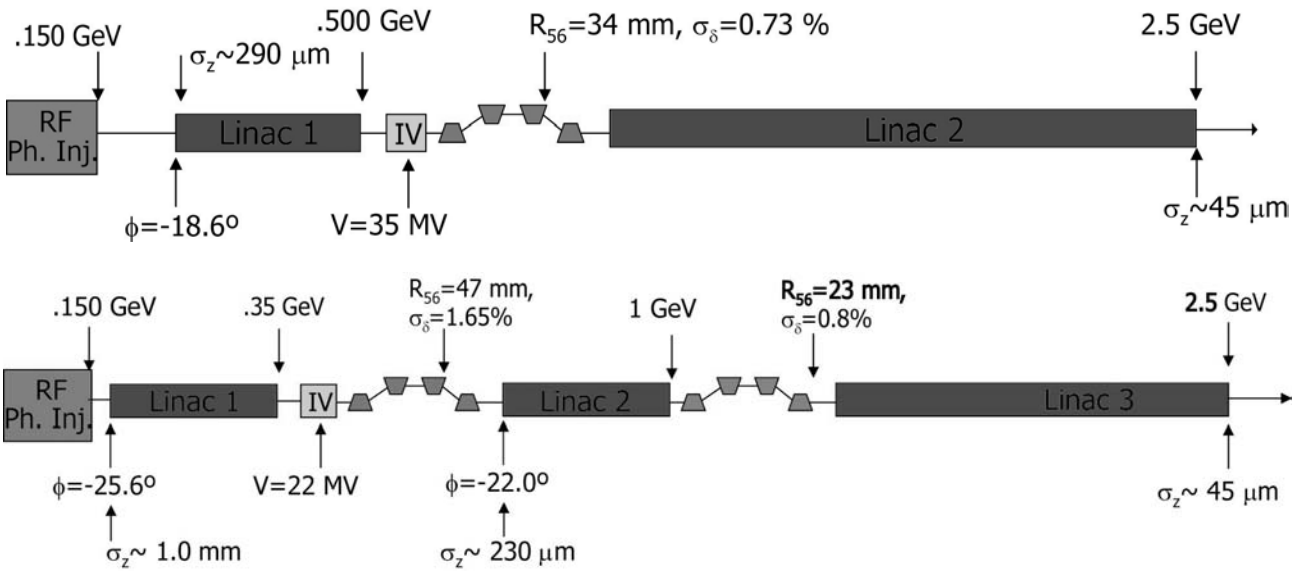

Figure 1: Schematic layout of the two SPARX linac designs: upper plot the Hybrid scheme, lower plot the Fully Magnetic scheme

HYBRID SCHEME

The PhotoInjector design considers a 1 nC bunch, 10 ps long (flat top) with a 1.2 mm radius, generated inside a 1.6-cell S-band RF gun of the same type of the BNL-SLAC-UCLA one, operating at 140 MV/m peak field equipped with an emittance compensating solenoid (B=3090 G). Three standard SLAC 3-m TW structures each one embedded in a solenoid boost the beam up to 150 MeV. Applying the RF compression method, together with the proper setting of the accelerating phase and solenoid strength it is possible to increase the peak current while preserving the beam transverse emittance [2]. We have obtained, (Parmela [3] simulation), a bunch average current of 300 A with a normalised rms emittance below 1 μm, as shown in figure 2, using the parameter setting listed in table 2.

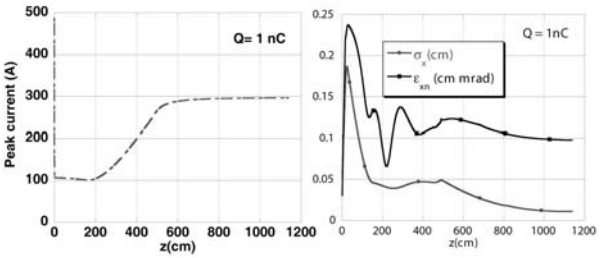

Figure 2: Parmela simulations of the peak current (left), rms norm.emittance and rms beam envelope (right), along the PhotoInjector structure.

Table 2

TW section	I	II	III
Gradient [MV/m]	15	25	25
Phase [Deg]	-86	-37	0
Solenoid field [G]	1120	1280	0

The Linac consists in a first accelerating section, Linac I, where 7 standard SLAC 3-m structures bring the beam up to an energy of .5 GeV. The accelerating phase is -18.6°, and the resulting energy spread is about 0.7%. A fourth harmonic cavity (11.424 GHz), follows, 60 cm long, in order to linearise the beam energy correlation. A magnetic chicane with R_{56} = 34 mm, about 15 m long, compresses the beam from 290 μm to 45 μm. A second accelerating section, Linac II , with 34 SLAC structures, in which the beam travels on crest, brings the beam energy up to 2.5 GeV and remove the energy spread .

FULLY MAGNETIC SCHEME

The PhotoInjector system consists of a 1.6 cell RF gun operated at S-band and high peak field on the cathode, (120 MV/m), generating a 6 MeV beam. The gun solenoid field is B=2730 G, and the injection phase is 33°. The beam is then focused and matched into 2 accelerating sections of the SLAC type, as described in [4]. Our simulations using PARMELA indicate that we can generate in this way a beam at 155 MeV with a rms correlated energy spread of 0.2%, and a rms norm. emittance of 0.6 μm (at 1.0 nC bunch charge and I = 90 A peak current). The slice energy spread and the slice norm. emittance, calculated over a 130 μm slice length, are well below 0.04% and 0.5 μm respectively, all over the bunch.

In the first accelerating section, Linac I, four standard SLAC 3-m structures bring the beam energy up to .35 GeV. The accelerating phase is -25.6°, and the resulting energy spread is about 0.17%. A fourth harmonic cavity follows in order to linearise the beam energy correlation. A magnetic chicane, about 3m long, with R_{56} = 47 mm compresses the beam from 1 mm to 230 μm. A second accelerating section, Linac II , with ten SLAC structures, operating at 22° off crest, accelerates the beam up to 1 GeV with energy spread 0.8%. The second chicane, R_{56} = 23 mm, 15 m long, compresses the beam up to 45 μm. In the third linac section, Linac III, twenty seven structures, accelerating the beam on crest, bring the beam energy up to 2.5 GeV and compensate the energy spread

TIMING JITTER ANALYSIS

One of the relevant aspects in the SPARX project is the sensitivity of the compression system to the laser pulse temporal jitter [5]. The performances of the two proposed schemes have been analysed and compared adding a 1° phase error at the RF gun injection stage.

The two channels have been optimized, with the code Litrack [6], to obtain the minimum sensitivity of the compressed beam properties to the phase error. For the hybrid scheme the optimized on has been performed on the channel downstream the RF compression stage, looking for the best combination of the relative phase of the first linac section, the X-band cavity voltage and the R_{56} value of the magnetic chicane. The same has been done for the purely magnetic channel regarding the parameters of the first two linac sections, the X-band and the two magnetic chicanes. The results are reported in table 3 and in figures 3 and 4. It's worth to notice that with the optimized Hybrid scheme in all of the three cases the final peak current is higher than 2 kA, and with the Purely Magnetic scheme, we have two cases with 2 kA and one with the peak current 10% lower.

Table 3

	Hybrid	**F. Magnetic**
Δϕ (ps)	I_{peak}(kA)	I_{peak}(kA)
0	2.0	2.0
+1	1.9	1.8
-1	2.4	2.3

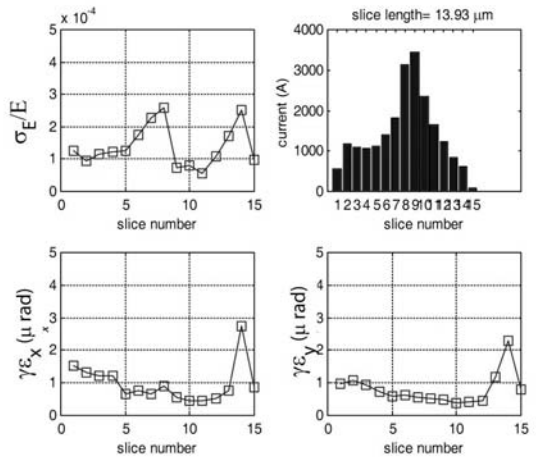

Figure 3: Slice analysis of the beam properties at the exit of the linac, for the hybrid reference case.

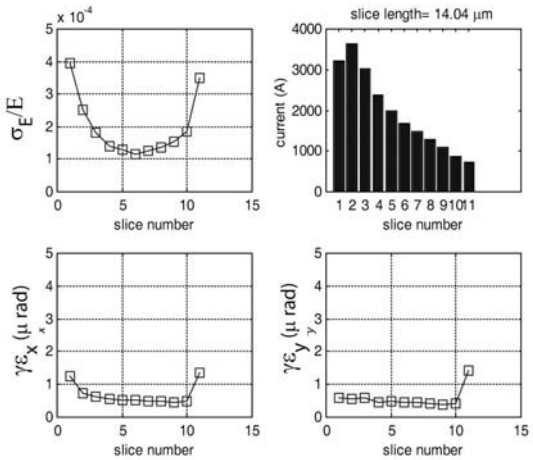

Figure 4: Slice analysis of the beam properties at the exit of the linac, for the fully magnetic reference case.

THE FEL SASE SOURCE

The beam quality has been tested by simulating the FEL process at the wavelength of 1.5 nm with the beam parameters obtained at the end of the last compression stage. The simulations have been done with the time dependent version of PERSEO [7]. The beam has been longitudinally "sliced" in five regions where the average parameters (emittance, energy, energy spread, current) have been calculated. The parameters of the slice with the higher current have been selected for the simulation. In table 4 a list of the "best slice" beam parameters for each case are shown. In table 5 the saturation length in presence of ±1° of phase jitter are reported for both schemes. The hybrid scheme with a phase jitter of +1° shows overcompression effects, resulting in more than 2 μm x-emittance. The magnetic saturation length is in this case of about 36 m.

Table 4

Case	I_{peak} (A)	ε_{nx}(m-rad)	ε_{ny}(m-rad)	γ	σ_E/E
Hybrid Reference	2790	0.83E-06	0.49E-06	4977	1.82E-04
Hybrid +1 °	2230	0.95E-06	0.51E-06	4982	5.53E-04
Hybrid -1 °	3330	2.13E-06	0.66E-06	4977	5.64E-04
Magnetic Reference	3237	0.84E-06	0.56E-06	5038	3.49E-04
Magnetic -1 °	2748	0.84E-06	0.62E-06	5038	2.80E-04
Magnetic +1 °	3744	1.10E-06	0.56E-06	5038	4.60E-04

Table 5

Case	Sat. L (m) (Steady State)	Sat. L (m) (Time Dependent)
Hybrid Reference	18.7	19.5
Hybrid +1 °	23.3	23.6
Hybrid -1 °	36.5	36.7
Magnetic Reference	18.5	19.0
Magnetic -1 °	19.6	20.5
Magnetic +1 °	19.9	20.2

CONCLUSIONS

We have analysed the effects of a phase jitter (±1°) on the SPARX beam quality considering two different concept for compression schemes,. The parameters have been set to obtain an equivalent compression factor between the two schemes. The slice parameters in terms of emittances, energy spread are comparable. The purely magnetic compression provides a more linearised longitudinal phase space which could in principle allow a further compression. We expect to obtain similar results also in the hybrid scheme with the IV harmonic cavity located upstream the RF compressor. The beam quality have been tested with time dependent PERSEO simulations showing a slightly lower sensitivity to phase jitter for pure magnetic compression. The low number of macroparticles considered in the ELEGANT simulations doesn't allow a correct representation of collective effects arising from the CSR coupling. A further effort in this direction is required to complete the analysis.

REFERENCES

[1] D. Alesini, et al. “Conceptual Design of a High-Brightness Linac for Soft X-ray SASE-FEL Source”, to be published on Nucl. Instr. and Meth. A
[2] M. Boscolo et al., proc EPAC02, p 1762, Paris 02
[3] J. Billen, “PARMELA”, LA-|UR-96-1835, 1996.
[4] M. Biagini et al., “Beam Dynamics studies for the SPARC project”, these conference
[5] P.J. Emma, proc. EPAC-02, p. 49 Paris 02.
[6] P.J. Emma , private communication
[7] L. Giannessi, http://www.perseo.enea.it

STUDY AND DESIGN OF ROOM TEMPERATURE CAVITIES FOR A RF COMPRESSOR PROTOTYPE

David Alesini[+], Franco Alessandria[*], Alberto Bacci[*], Carlo De Martinis[*] , Massimo Ferrario[+], Alessandro Gallo[+], Dario Giove[*], Fabio Marcellini[+], Marco Mauri[*], Luca Serafini[*]

[+]*INFN-LNF-Frascati* , [*]*INFN-Milan and University of Milan*

Abstract

The generation of high brightness electron beams with sub-ps bunch lentgh at kA peak currents is a crucial requirement in the design of injectors for Linac based X-Ray FEL's. In the last years the proposal to use a slow wave RF structure as a rectilinear compressor in this range of interest, to overcome the difficulties related to magnetic compressors, has been widely discussed in the accelerator physics community. In this paper the results in the design and study of a 3 GHz model structure will be presented.

INTRODUCTION

The need to produce high brightness electron beams delivered in short (sub picosecond) bunches has been driven recently by the demands of X-Ray SASE FELs, which require multi-GeV beams with multi-kA peak currents and bunch lengths in the 100-300 fs range, associated to normalized transverse emittances as low as few mm mrad. The strategy to attain such beams is based on the use of RF Linacs in conjunction with RF laser driven photo-injectors and magnetic compressors. The formers are needed as sources of low emittance high charge beams with moderate currents, the latter are used to enhance the peak current of such beams up to the design value of 2-3 kA by reduction of the bunch length achieved at relativistic energies (> 300 MeV). Nevertheless the impact of magnetic compressors on the beam dynamics is quite relevant, with tendency to reduce the performances of the whole system in terms of the final beam brightness achievable [1].

In the last years, developing a previous work about a plasma buncher scheme, alternative option of compression based on slow wave RF fields has been proposed [2]. The basic idea is to develop a rectilinear RF compressor that works indeed as a standard accelerating structure which simultaneously accelerates the beam and reduces its bunch length.

RF RECTILINEAR COMPRESSOR THEORY

The great advantage of a rectilinear scheme is obviously the absence of curved path trajectories, in addition to the fact that compression is applied at moderate energies (from 10 to 100 MeV) leaving the Linac free from any further beam manipulation.

We briefly report the basic elements of the theory of RF compressor as outlined in ref.2.

The interaction between an electron and the longitudinal component E_z of the RF field in a RF travelling wave structure is described by the Hamiltonian

$$H = g - b_r\sqrt{g^2 - 1} - a\cos x$$

where $g = 1 + \frac{T}{mc^2}$ is the normalized energy of the electron, $x = (wt - kz - y_0)$ is the phase of the wave as seen by the electron (y_0 is the injection phase) and $a = \frac{eE_0}{2mc^2k}$ is a dimensionless parameter which represents the accelerating gradient.

If we consider a wave whose phase velocity is slightly lower than c, we have that $k = k_0 + \Delta k = \frac{w}{c} + \Delta k$ (where the detuning parameter is small i.e. $\Delta k << k_0$) and we can write for the resonant beta and gamma the expressions $b_r = 1 - \frac{c\Delta k}{w}$ and $g_r = \sqrt{\frac{w}{2c\Delta k}}$.

The behaviour of the RF compressor may be easily understood looking at the phase contour plots in the [?,?] phase space. As an example we have considered a wave of amplitude a = 0.65 and resonant gamma $?_r$ = 24. This corresponds to a wave phase velocity of b_r =0.999.

In fig. 1 we plot a phase-space diagram showing that particles injected with a phase equal to –p/2 and an energy smaller than the resonant one, will slip back in phase while accelerated up to ? = $?_r$. Due to the nature of phase lines the bunch will have a phase spread (i.e. a bunch length) smaller than the initial one. For the same reason a further acceleration would clearly tend to de-compress the bunch.

The figure of merit for the compression process may be defined as the ratio between the initial phase spread and the final one at the extraction. Values in excess of 10 may be reached in such a scheme. A proper matching of the beam into the accelerating section and an additional focusing provided by external solenoids has been shown by simulation to obtain a proper preservation of the transverse emittance as discussed in Ref. [3]

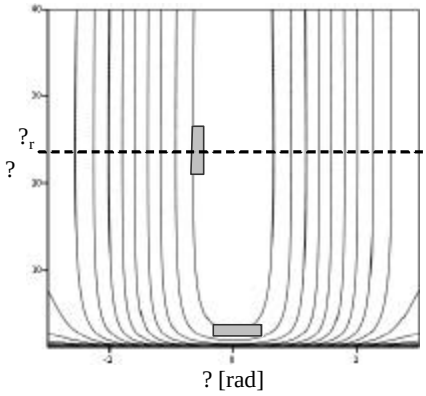

Fig. 1 Phase space plots of a slow RF wave

DESIGN OF CELLS FOR A SLOW WAVE RF COMPRESSOR

In the last year preliminary experimental investigations have been carried out using speed of light linac sections, which showed the validity of the velocity bunching concept[3]. In such a frame our group started an experimental activity aimed at the development of cells for the construction of a slow wave TW structure which can be used as a RF compressor. Table 1 shows the main parameters which we took as a reference for our investigations:

Parameter	Value
Frequency of the wave structure	2856 MHz
Linac structure	TW
Accelerating gradient	20 MV/m
Initial energy	6 MeV
Extraction energy	16 Mev
Compression factor	7
RF pulse repetition rate	1÷10
Bunch length	10 ps

Table 1 Reference parameters for the study of the RF compressor

The required compression factor calls for the availability of a structure able to control the phase velocity in the range between 0.999 c and c. In an iris loaded TW structure the equation:

$$(dvf / vf) = (df / f) (1 - vf / vg)$$

shows that the v_f can be controlled by changing the excitation frequency or, in a equivalent way, by detuning the structure. A suitable approach may be that to use a thermal control process that change the v_f at a fixed exciting frequency. The feasibility of such an approach has been initially studied referring to the typical parameters of a SLAC structure. The results obtained show that a change of the order of 1‰ of the phase velocity is equivalent to a variation of the order of 0.6 °C in the temperature of the structure. This calls for a system able to control in real time the temperature with a resolution of the order of 0.06°C under a RF power load of the order of ~ 1.5 kW. We evaluated that it would be too much difficult to achieve such a performance and we tried to approach the problem with a new cell design. The goal was to obtain a structure able to decrease of a factor of 3 the thermal sensitivity, so that the required phase velocity modulation will ask for a temperature variation of the order of 2 °C. The fact that the required accelerating gradient is lower with respect to a standard SLAC structure gave us a certain degree of freedom in the design as far as the shunt impedance figure is involved. Table 2 shows the main parameters of the new structure (referenced as ALMA 3) which we propose for the RF compressor:

	SLAC Mark IV	Alma 3
Cell radius (mm)	41.24	42.60
Iris radius (mm)	11.30	15.40
Disk thickness (mm)	5.84	5.90
Cell length	35	35
Frequency (MHz)	2856	2856
Mode	2π/3	2π/3
Q	13200	13084
Shunt impedance (MOhm/m)	53	41
Vg/c	0.0122	0.0341
?T (equivalent to 1‰ Vf)	0.6 °C	2.0 °C
Tuning ring capability (MHz)	-	18
Tuning rod capability (kHz)	-	200

Table 2 Main parameters of the Alma 3 TW structure

The mechanical design of the cell has been carried out in a complete fashion taking into account the requirements due to the cooling system and to the brazing process to join cells to give the final structure.

At the same time, at least for the first prototypes, we add frequency control capabilities to the cells both during the mechanical machining (using a tuning ring) and after the brazing (using a set of tuning rods). Such a feature has been foreseen to allow to control the influence of the achievable mechanical tolerances on the frequency response of the cells (a tolerance of 0.01 mm in the cell diameter gives an uncertainty of 370 kHz in frequency) and to provide a tuning tool for field adjustment.

The thermal control of this structure will be obtained using 8 channels for water flow. These channels have been machined within the cells body to provide a better heat exchange. The behaviour of this design has been verified under the expected RF power load using the finite element code Ansys. The results of this analysis show that the system will be suitable to match our requirements (fig. 2). The so far obtained thermal sensitivity allows to use a refrigeration unit with a control capability of the order of 0.1°C@45°C operating point. Such units are commercially available and we plan to use one of these as the basic building block of the thermal control setup.

To prove the reliability of the design and to gain experience on such a structure we machined a 4 cells aluminum prototype. The cells were stacked together using stainless steel threaded rods.

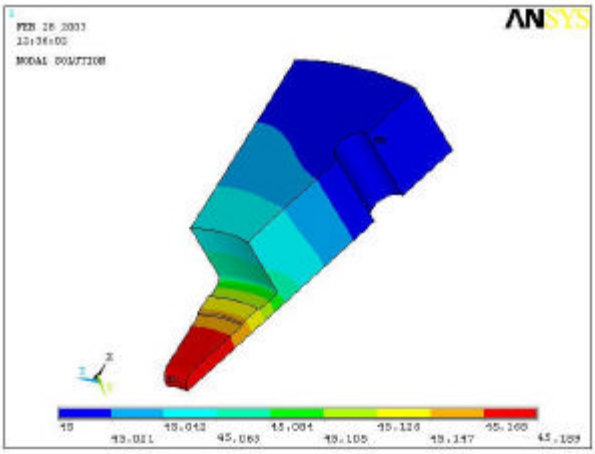

Fig. 2 Ansys simulation of the thermal behaviour of the ALMA 3 structure

The machining of these cells was simplified with respect to the final ones removing the cooling channels and the brazing grooves. The mechanical tolerances obtained were quite close to those required and this allowed to carry out significant measurements both on the single cell and on the set of the four cells.

The resonant frequency measurements on the single cells were in very good agreement with the expected values obtained with the code Superfish and confirmed the influence of the mesh value adopted in the numerical analysis (0.15 mm which gave us a frequency accuracy of the order of 100 kHz). For the sake of simplicity we started considering this assembly as a SW structure giving us the opportunity of sampling the dispersion curve at 4 points and to check field profile (Fig. 3).

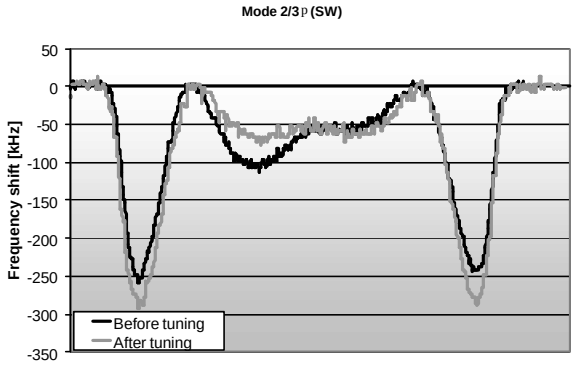

Fig.3 Measurements of the ALMA 3 structure accelerating field

The dispersion curve as a function of the cells temperature was measured using a test bench based on a laboratory oven. The internal size of the oven allows to position the 4 cells stack along with RF probes and temperature sensors to characterize the oven behaviour and to measure the cells temperature. Measurements were carried out in the range between 25 and 45 °C. The oven stability was of the order of 0.1 °C. The results (Fig. 4) proved a good agreement with the predicted behaviour of the phase velocity and gave the final validation of the whole design.

At the same time that we carry out the above described measurements, the OFHC copper to be used for the machining of a new 9 cells prototype has been forged by an Italian company according to our specifications. Great care has been taken to the control and measurement of the grain size of the bulk material (< 100 µm) in order to match the requirement for the brazing procedure. This process will be carried out at CERN and the whole cycle has been defined in agreement with CERN specialists.

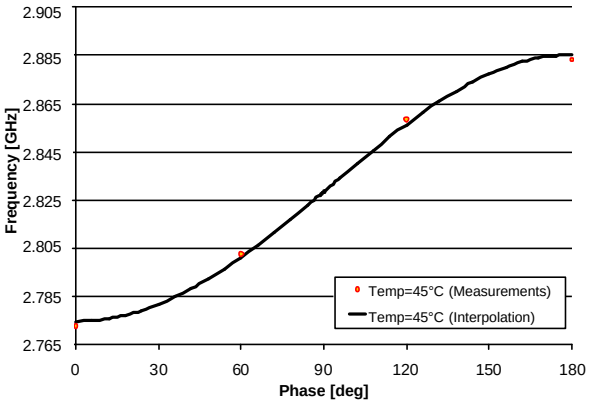

Fig. 4 Measurements of the ALMA 3 structure dispersion curve

CONCLUSIONS

The design of a new cell for a RF compressor working in the S-band has been completed and the measured performances of a first aluminum prototype have proven the feasibility of such an approach.

At this time the machining of the copper cells has been started and we plan to have a 9 cells brazed structure within the end of June 2003.

ACKNOWLEDGEMENTS

We would like to acknowledge very helpful discussions with M. Vretenar and S. Mathot (CERN), R. Boni (INFN-LNF) and the valuable support received in the experimental work by Luigi Gini and Carlo Uva (INFN-Milan) and Luciano Grilli (University of Milan).

REFERENCES

[1] P.Emma "Accelerator Physics Challenges of X-Ray FEL SASE Sources", EPAC2002, Paris, June 2002, p. 49

[2] L. Serafini et al. "Ultra-short Bunch Generation with a Rectlinear Compressor", PAC2001, Chicago, June 2001, p. 2242.

[3] M. Ferrario et al. "Recent Advances and Novel Ideas for High Brightness Electron Beam Production Based on Photo-Injectors" INFN-LNF 03/06P– 5 May 2003

SELF-CONSISTENT 3-D PIC CODE FOR MODELING OF HIGH-BRIGHTNESS BEAMS

Alberto Bacci, Cesare Maroli, Vittoria Petrillo and Luca Serafini

INFN-Milan and University of Milan

Abstract

The 3D numerical code RETAR has been developed to model the beam dynamics of high-brightness electron beams in photoinjectors and in magnetic compressors, where the interaction of the beam with its self-field is of crucial relevance to optimize the performances of these devices, either in the case of space charge dominated dynamics or under strong coherent synchrotron radiation effects, respectively. The code is fully relativistic and calculates the self-fields directly from convenient integral forms that can be obtained from the usual retarded expressions. Numerical results are presented so far for the dynamics of an electron bunch in a radio-frequency photo-injector taking into account solenoidal magnetic focusing fields, RF focusing, thermal emittance, image charges inside the cathode surface, acceleration and space-charge effects.

INTRODUCTION

RETAR is a 3D code for the description of the motion of an electron beam under any kind of (given) external electromagnetic (em) fields plus the fields created by the beam itself (space-charge and radiation-fields). At the present time, the code is limited to consider only propagation in vacuum. Metallic or other kind of boundaries will be added in the future.

The trajectory of each single electron of the beam satisfies the following equations:

$$\frac{d\mathbf{x}_j}{dt} = \mathbf{v}_j \quad ; \quad \frac{d\mathbf{p}_j}{dt} = -e(\mathbf{E}_{tot} + \frac{\mathbf{v}_j}{c} x \mathbf{B}_{tot})$$

where $\mathbf{E}_{tot}$ and $\mathbf{B}_{tot}$ are the total fields acting on each electron, taking into account both external and self fields. The equations of motion are integrated by means of a second-order Runge-Kutta scheme: this does not cause any particular difficulty provided all forces acting on the electrons are known at each time step. The electron itself is actually a *macro-electron*, with total charge and mass that are several orders of magnitude larger than the charge and mass of a true electron. These macro-electrons are considered as point like particles but their number everywhere within the bunch is supposed to be sufficiently large as to allow suppression of divergent or very large contributions to the em self-fields, when they happen to be calculated at points very near to the electrons or exactly on the electrons. As regards the external forces, they are obviously considered to be known as functions of time and everywhere within the region of space crossed by the beam in its motion outside the cathode surface. The em self-fields are calculated directly (*i.e.* without calculating first the em potentials) in terms of the values of the charge density $\rho(\mathbf{x},t)$ at time t and at all preceding times, through the following equations that can be readily obtained by an easy manipulation of the usual retarded forms

$$\mathbf{E}(\mathbf{x},t) = \int d\mathbf{x}' \rho(\mathbf{x}',\tau) \mathbf{Q}_{\mathbf{E}}(\mathbf{x}-\mathbf{x}',\tau) \qquad (1)$$

$$\mathbf{B}(\mathbf{x},t) = \int d\mathbf{x}' \rho(\mathbf{x}',\tau) \mathbf{Q}_{\mathbf{B}}(\mathbf{x}-\mathbf{x}',\tau) \qquad (2)$$

where $\tau = t - \frac{1}{c}|\mathbf{x}-\mathbf{x}'|$ and

$$\mathbf{Q}_{\mathbf{E}} = \frac{\mathbf{n}-((\mathbf{n}-\boldsymbol{\beta})\cdot\dot{\boldsymbol{\beta}})}{c|\mathbf{x}-\mathbf{x}'|(1-\mathbf{n}\cdot\boldsymbol{\beta})^2} + \frac{(\mathbf{n}-\boldsymbol{\beta})(1-\mathbf{n}\cdot\boldsymbol{\beta})^2}{\gamma^2|\mathbf{x}-\mathbf{x}'|^2} \qquad (3)$$

$$\mathbf{Q}_{\mathbf{B}} = -\frac{\mathbf{n}\times(\dot{\boldsymbol{\beta}}(1-\mathbf{n}\cdot\boldsymbol{\beta}) + \boldsymbol{\beta}(\mathbf{n}\cdot\dot{\boldsymbol{\beta}}))}{c|\mathbf{x}-\mathbf{x}'|(1-\mathbf{n}\cdot\boldsymbol{\beta})^2} - \frac{(\mathbf{n}-\boldsymbol{\beta})(1-\mathbf{n}\cdot\boldsymbol{\beta})^2}{\gamma^2|\mathbf{x}-\mathbf{x}'|^2} \qquad (4)$$

In addition, $\mathbf{n} = (\mathbf{x}-\mathbf{x}')/|x-x'|$, $\boldsymbol{\beta} = \mathbf{v}(t)/c$, and all time dependent quantities in (3) and (4) are calculated at the retarded time τ.

The 3D integrals in (1) and (2) are calculated in the following way:

i) The whole space around the point $\mathbf{x}$ at which the fields are to be computed, is divided into a set of spherical shells of a conveniently small thickness .

ii) In each shell the code sums the values of the vector $\mathbf{Q}_{\mathbf{E}}$ (and those of $\mathbf{Q}_{\mathbf{B}}$) at all points that happen to be occupied at the corresponding retarded time by one of the electron of the beam. The retarded time itself depends only on the radius of the shell and is the same everywhere inside each shell.

iii) The integrals giving the electric field $\mathbf{E}$ and the magnetic induction $\mathbf{B}$ at the position $\mathbf{x}$

and time t, are then obtained by summing the contributions from all spherical shells.

The basic advantages of this method seem to consist in i) the absence of convergence difficulties that may arise when one chooses to calculate the em self-fields from direct numerical integration of the relevant propagation equations and ii) in the fact that the retardation is very simply taken into account instead of having to find by means of a Newton iteration, for instance, the root of a complicated equation, when one chooses to calculate the em self-fields by summing the fields produced by each single electron as given by the Liénard-Wiechert equations. The CPU time is expected to scale as the product of the number of macro-electrons times the number of spherical shells, implying a linear scaling with the number of macro-electrons: we are in the process of checking in details this scaling law which represents a clear advantage over particle-to-particle integral codes based on Liénard-Wiechert retarded potentials.

The values of the self-fields obtained inside and outside the electron beam have been accurately tested by comparing them with well-known analytical and numerical estimates in various situations where space charge field is dominant (cylindrical and elliptic cross-section bunches with relativistic velocities) and the results have always shown fairly good agreement.

This algorithm is fully self-consistent in a 3D fashion, so it is suitable for the study of a class of beams strongly interacting with space charge and radiation fields: since it is based on an integral description for the field components, there is no mesh discretization, hence no limitations arising from space discretization of the field propagation like in case of differential PIC codes. Time (frequency) and space resolutions are only set by the number of spherical shells used in the simulation to reconstruct the retarded times.

NUMERICAL RESULTS

We are applying the code to the specific purpose of simulating numerically the relativistic motion of the electrons that are emitted by short laser pulses from the photo cathode surface and immediately subjected to a strong acceleration and focusing by suitable given electromagnetic fields.

The analysis includes the self-fields of the electrons that leave the cathode, as well as the fields produced by the image charges inside the cathode. The electron injection is simulated by fixing the electron flux at the cathode surface (for instance the plane $z = 0$), *i.e.* by giving the number of electrons streaming out of the cathode per time interval and surface element. Thermal fluctuations in both spatial locations and velocity distribution of the electrons emitted are taken into account.

The photoinjector lay-out considered in these simulations is that of SPARC, described in a separate paper [1]: the external magnetic field has a solenoidal shape with the maximum value $B_z = 0.27\ T$ on the axis at $z = 20$ cm, while the axial component of the electric field is applied with a peak field on the cathode $E_0 = 120\ MV/m$. The beam is accelerated in the RF gun up to about 6 MeV and propagated along 1.2 m of downstream drift space. 2000 macro-electrons and 100 spherical shells have been used in this simulation with an integration time step of 0.5 ps : the CPU time was about 3 hours on a 1.8 Ghz processor.

In Figure 1 the time evolution of the beam is presented at different times. Significant values of the beam parameters are: the total beam charge $Q = 1\ nC$, the laser pulse length 10 ps (uniform flat top time distribution for the laser pulse intensity), initial beam radius $R = 1$ mm, initial thermal emittance $\varepsilon_n = 0.3$ mm, launching phase 30 °RF.

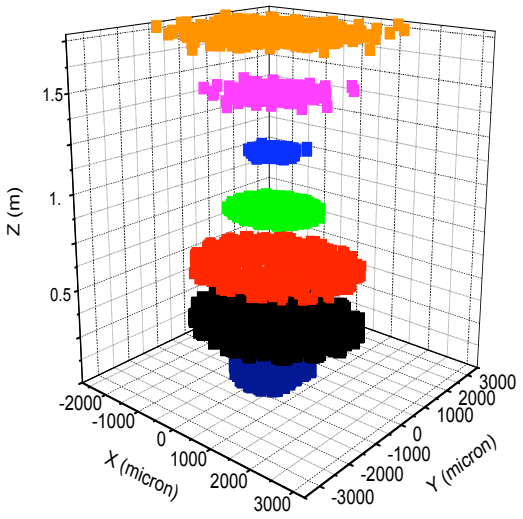

Figure 1: temporal evolution of the beam through the SPARC photoinjector

In figure 2 the rms radius σ_r and the rms normalised emittance:

$$\varepsilon_x = \sqrt{< x^2 >< p_x^2 > - < xp_x >^2}$$

are plotted as functions of z for the values of the parameters given previously showing that the minimum value of ε_x takes place at $z = 105$ cm in correspondence of the minimum of the rms radius.

No systematic investigations has been done yet on the optimum parameter set in order to minimize the emittance according to the Ferrario criterium for the working point of integrated photo-injectors [4]. Therefore, the

comparisons to other simulations are quite preliminary, with the aim just to test the absence of errors in the code.

In Figure 3 the $r - p_r$ phase space is shown at the same time instants as in Figure 1.

After the focusing, a degradation of the beam quality can be seen, apparently due to non linear space charge effects in combination to an incorrect matching into the invariant envelope [3,4] conditions.

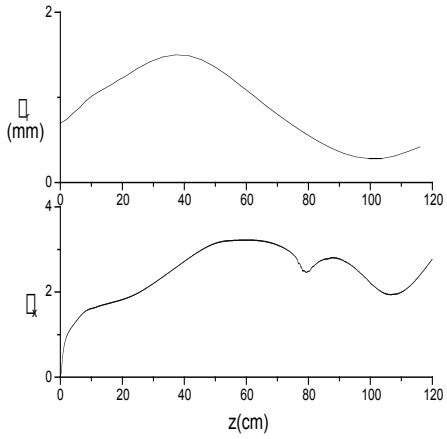

Figure 2: rms radius σ_r in mm and normalised emittance ε_x in μm vs z in the case of SPARC parameters

The RETAR code has been compared with other beam evolution codes as for instance Homdyn [2] based on the envelope approximation [3].

In Figure 4 the comparison between the average kinetic energy as given by RETAR (black curve) and Homdyn (red curve) for the same parameters is shown for the first 12 cm.

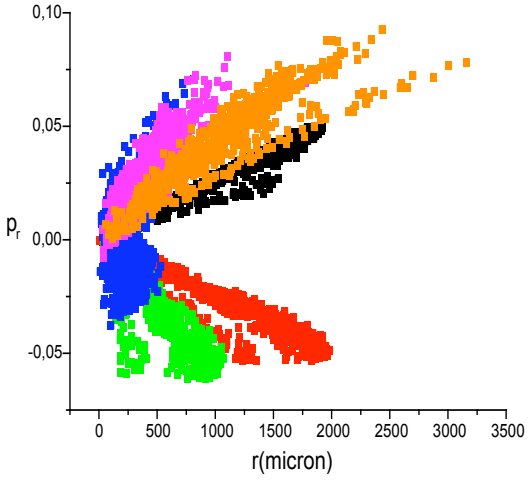

Figure 3:beam evolution in the $r - p_r$ phase space

As for the beam envelope and the rms transverse emittance, we found a slight discrepancy with Homdyn, which predicts an emittance minimum located at 1.5 m with a minimum value of 0.6 μm. We believe most of this discrepancy is due to an incorrect setting of the most critical parameters (solenoid peak field, launching phase, cathode spot size) and we are in the process of investigating it thoroughly.

In conclusion, the code RETAR is under test in the context of a class of general beam phenomena where beam-field interaction is of crucial relevance: we reported here the preliminary results of testing the code in photoinjector beam dynamics. Next step will be the study of CSR effects in magnetic compressors.

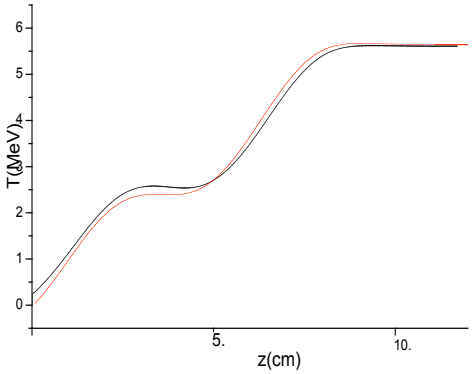

Figure 4: comparison between RETAR and Homdyn

REFERENCES

[1] M. Biagini *et al.*, *Beam Dynamics Studies for the SPARC Project*, this conference

[2] M. Ferrario *et al., Particle Accelerators* **52** (1996) 1

[3] L. Serafini, J.B. Rosenzweig : Phys.Rev. E **55** (1997) 7565

[4] M. Ferrario *et al., Recent Advances and Novel Ideas for High Brightness Electron Beam Production based on Photo-Injectors*, INFN Rep. LNF-03/06 (P), May 2003

CODE COMPARISON FOR SIMULATIONS OF PHOTO-INJECTORS

C.Limborg[*], Y.Batygin[*], M.Boscolo[•], JP.Carneiro[♣], M.Ferrario[•], K.Floetmann[♣],

V. Fusco[•], L.Giannessi[♦],C.Ronsivalle[•], M.Quattromini[♦]

([*]) MS 69 SLAC 2275 Sand Hill Road, Menlo Park , 94025 CA, USA

([♣])DESY, Notkestrasse 85, 22603 Hamburg, Germany

([•])INFN-LNF, Via E. Fermi 40. I-00044, Frascati (Roma), Italy

([♦])ENEA Research Center Via Enrico Fermi 45, 00044 Frascati (Roma), Italy

Abstract

RF photo-cathode injectors constitute one of the key components of many future single pass FEL based synchrotron radiation sources. The possibility of reaching very high brightness beams had been anticipated by using various simulations tools. Several experiments have proven that the 1mm.mrad normalized projected emittance for 1 nC, 10 ps pulses is within reach. For optimizing these photo-injectors, a first search of parameters is efficiently performed with HOMDYN. Further refinement in the tuning is usually obtained using a multi-particle tracking code such as ASTRA, PARMELA or BEAMPATH. In this paper, we compare results from HOMDYN, ASTRA, PARMELA, and BEAMPATH for the cases of an S-Band photo-injector. Limitations in their accuracy and differences between the codes are discussed.

1- MOTIVATION

Many codes are available for studying the dynamics of intense electron bunches at low energy in the space charge dominated regime. Newcomers in the field often ask which code to use to start studying a system based on a photo-cathode RF gun. In this paper, we compare codes which use five very different algorithms to compute the space charge: a code which solves the envelope equation HOMDYN [1], a Cloud-In-Cell (CIC) code BEAMPATH [2], a ring based algorithm PARMELA[3] and ASTRA[4], a fast Particle-In-Cell (PIC) algorithm for PARMELA spch3d and and a Lienard-Wiechert potentials approach for TREDI [5]. The test problem studied consists in an S-Band RF gun, a compensation solenoid and a drift. Quantities of interest such as rms beam size, emittance bunch length could be matched for all those codes when optimal running conditions.

2- DESCRIPTION OF CODES

HOMDYN

HOMDYN relies on a multi-envelope model based on the time dependent evolution of a uniform bunch[1]. The basic approximation, in the description of the beam dynamics, lies in the assumption that each bunch is represented by a uniformly charged cylinder whose length and radius vary, assuming a uniform charge distribution inside the bunch. The HOMDYN algorithm is very efficient and despite some strong simplifying assumptions it allows the quick relaxation of the large number of parameters involved in parameter studies, to quickly find a reasonably optimized configuration.

BEAMPATH

BEAMPATH is used for 2D and 3D simulation of axial-symmetric, quadrupole-symmetric and z-uniform beams in a channel containing RF gaps, radio-frequency quadrupoles, multipole lenses, solenoids, bending magnets, and user-defined elements. The space charge potential of the beam is calculated from the direct solution of Poisson's equation by cloud-in-cell method in a moving system of coordinates with Dirichlet boundary conditions at the aperture and periodic conditions in z-direction. Simulation of the beam with large energy spread is performed utilizing Green function method for interaction of particles with individual energies. To simulate particle emission in RF photoinjector, the code was updated by an additional space charge routine which solves Poisson's equation inside a cylindrical iron box. This approach automatically takes into account image charges arising both from injection plane and from surrounding aperture.

PARMELA / ASTRA

PARMELA and ASTRA compute the space charge force by Lorentz-transforming the particles positions and field maps into the average rest frame of the beam. It then applies static forces to the various rings of the cylindrical map assuming a constant charge density inside a ring. This algorithm requires to have at least 5 particles in each of the cell of the cylindrical grid.

PARMELA /SPCH3D

The SPCH3D algorithm of PARMELA-LANL is based on a fast Fourier Transform set on a 3D grid over which the electric field is solved to verify Poisson’s equation [6].

It is quite time consuming as it requires running at least 100k particles and small aspect ratios of the cell dimensions. This algorithm is nevertheless necessary to be used when the aspect ratio horizontal to vertical of the beam is more than 2 and when the transverse profile does not have a cylindrical symmetry. The automated remeshing is included when using this algorithm.

TREDI

TREDI is a fully three dimensional Monte Carlo code devoted to the simulation of beam dynamics. Space charge fields can be evaluated in a point to point or point to mesh & interpolation mode, calculating the fields according to the Lienard Wiechert formalism and taking into account the effects due to the finite propagation velocity of signals. This is accomplished by storing the histories of macro-particles, and by tracking back in time the source coordinates until a retarded condition is fulfilled. Short bunch injector simulations (as the test case) can be run also in a faster "Static" mode, where instantaneous signal propagation is assumed. The "Retarded" mode allows the simulation of a wider class of problems such as CSR effects in bendings.

3- PROBLEM DESCRIPTION

The test problem consisted of simulating a S-Band gun with an emittance compensation solenoid and a drift for a 10ps square pulse, 1 mm uniform transverse laser pulse producing a 1 nC charge. No thermal emittance was included. The solenoid was set to 2.541 kG.

The first difficulty in performing such comparisons consists in implementing exactly the same maps of fields (electromagnetic for the gun field and magnetostatic for the solenoid). All of the five codes studied can translate outputs from SuperFish and Poisson. So identical maps were used. The second difficulty consists in using the same starting conditions. Each of the codes has its own launching conditions. To check that starting parameters were in agreement for all codes, we compared energy and beam sizes output for cases run without space charge. A very good overlap was obtained with the 5 codes. We could then study the single impact of the different space charge algorithms.

4- RESULTS OF COMPARISONS

Good agreement inside gun

The rms quantities beam size, emittance, bunch length and energy spread could be matched exactly for all the 5 codes inside the gun. The rms beam size obtained at the gun exit was slightly smaller with HOMDYN, see figure 1. The differences become larger in the drift which follows.

Some disagreement in drift

The local maximum in emittance around 1.5 m shows at 1.2 m in HOMDYN but around 1.5 for all the other codes, See figure 2. The first local emittance minimum is nearly identical for the multiparticle codes and the agreement is not as good for the second minimum. The energy spread from HOMDYN is closer to that of the other codes if only the core slices are taken into account for the comparison.

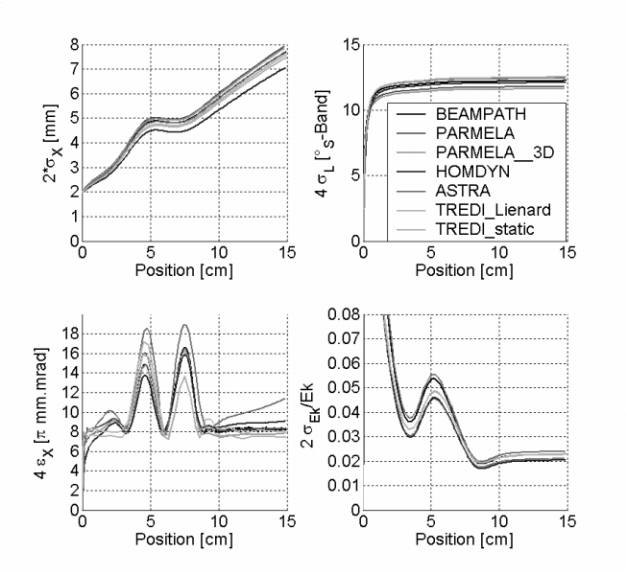

Figure 1.Comparison of evolution of rms beam size, bunch length, emittance and energy spread inside gun for the 5 codes

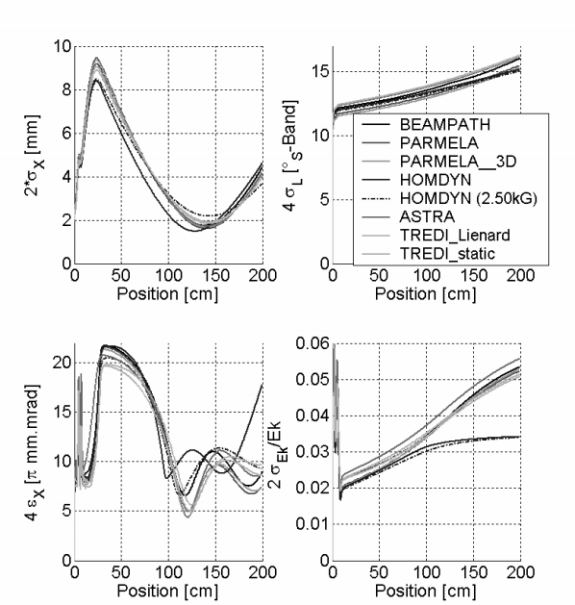

Figure 2.Comparison of evolution of rms beam size, bunch length, emittance and energy spread up to 200 cm for the 5 codes; second HOMDYN case run with solenoid reduced from 2.541kG down to 2.5 kG

5- MESHING IN TIME AND SPACE

Results depend strongly on the meshing used for the CIC code and for the SCHEFF algorithm. As a rule of thumb, each mesh should contain about 5 particles.

Table 1 – Comparison CPU time

Code	Platform	CPU	Num. particles	Mesh points N_r x N_z	Mesh size h_r x h_z	Integration step	CPU time (s)
HOMDYN	PC Win		75 slices			0.13 ^{o}	45
BEAMPATH	PC Win	1 GHz	10^4	256 x 2048	50x50μm^2	0.1^o , 1^o	8000
PARMELA	"	1 GHz	2.5 10^4	25 x 75	"	"	9846
" spch3d	"	1 GHz	10.10^4	32 x 32 x 1024	Automatic	"	1.4.10^4
ASTRA	"	1.8 Ghz	1.5 10^4	20 x 60	Automatic	Adaptative	420
Tredi Stat.	16 nodes	1.8 GHz	5.0 10^4	20 x 30	Automatic	Adaptative	7.5 10^3
Tredi Lien.	PC Win	1.8 GHz	5.0 10^4	20 x 30	Automatic	Adaptative	7.4 10^4

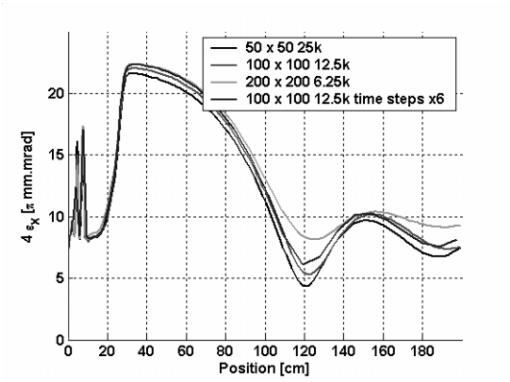

Figure 3. PARMELA results for the different meshes described in Table 2; Only the emittance varied for those 4 different cases, other parameters stayed constant

Table 2: PARMELA CPU Time on 1GHz PC

time	**SPACE Mesh.**	**TIME Mesh.**	**Particles**
9846 s	50 x 50 μm^2	1100, 0.1° then 1°	25 k
1286 s	100 x 100 μm^2	1100, 0.1° then 1°	12.5 k
445 s	200 x 200 μm^2	1100, 0.1° then 1°	6.25 k
345 s	100 x 100 μm^2	505, 0.2° then 1°	12.5 k

6- PHYSICS REPRESENTED

INITIAL ACCELERATION

A comparison of the dynamics between PARMELA and PIC codes [7], has shown that:

1- the image charge model is good enough to represent the boundary conditions at the origin
2- the computation of space charge forces, performed in the frame of the center of mass of the bunch in PARMELA type codes, when the Lorentz factor is small give good enough results compared with PIC or Lienard-Wiechert codes
3- neglecting the radial force generated from the beam self-induced azimuthal magnetic field does not affect the results

It was confirmed with BEAMPATH and TREDI that the approximation described in the second is correct. In TREDI the approximation is simply not used and BEAMPATH can perform computations using a Poisson solver for which individual energies are taken into account. The use of this solver for the first few mm is very time consuming but did not change the results at the end of the gun.

THERMAL EMITTANCE

In each of these codes the initial distribution can be given such that a thermal emittance is included. None of the codes include the physics involved in the generation of that thermal emittance. This is one of the key issues of the RF-Cathode gun to be tackled.

SHOTTKY EFFECT

ASTRA is the only code which includes this effect.

LONGITUDINAL PROFILE

Each of the codes can include the rise and fall time of the initial pulse but HOMDYN.

TRANSVERSE NON-UNIFORMITY

When the transverse profile does not have cylindrical symmetry, only 3D space charge algorithm should be used as in TREDI or PARMELA in the spch3d mode. ASTRA is being upgraded to offer a similar possibility.

PARMELA-UCLA and PARMELA-LANL include the possibility of using 3D maps of fields. It was checked [7] that the quadrupole moment present in the S-Band gun to be used for LCLS has negligible effects in the dynamics of the beam.

REFERENCES

[1] M.Ferrario, HOMDYN code : http://www.slac.stanford.edu/pubs/slacpubs/8000/slac-pub-8400.html

[2] Y.Batygin, "Particle-in-cell code BEAMPATH for beam dynamics simulations with space charge", ISSN 1344-3877, RIKEN-AF-AC-17 (2000), 81 p.

[3] L.Young, J.Billen , PARMELA, LANL Codes, laacg1.lanl.gov/laacg/services/parmela.html

[4] K.Floetmann,ASTRA, http://www.desy.de/~mpyflo/Astra_dokumentation/

[5] F. Ciocci, L. Giannessi, A. Marranca, L. Mezi, M. Quattromini, Nucl. Instr. & Meth. A 393, 434 (1997)., Web site: http://www.tredi.enea.it

[6] R.Ryne et al., Proc. 1998 Linac Conf., Chicago,IL

[7] E.Colby, et al."Simulation Issues for RF Photoinjectors" 7th Computational Accelerator Physics Conference, Michigan State U. Oct15-18-2000

*limborg@slac.stanford.edu

SLAC is operated by Stanford University fot the Department of Energy under contract number DE-AC03-76SF00515

STUDY OF A LOW IMPEDANCE BEAM POSITION MONITOR FOR SHORT BUNCHES

D. Alesini, B. Spataro, C. Vaccarezza, LNF-INFN, Frascati (Rome), Italy
C. D'Alessio, A. Mostacci, L. Palumbo, University "La Sapienza", Rome, Italy

Abstract

A low coupling impedance beam position monitor based on microwave spectroscopy is proposed. A coaxial cavity is coupled to a circular beam pipe through four small longitudinal slots. Displaced beams excite TE cavity modes that can be detected by two antennas. Applying the modified Bethe's theory, the TE_{111} mode power has been derived as a function of the beam displacement. An aluminium prototype has been constructed with the support of numerical (HFSS) simulations. Bench measurements using a coaxial wire excitation show good agreement with both theoretical and numerical expectations.

1 INTRODUCTION

Different methods to measure beam position inside the pipe have been proposed either in the time domain than in the frequency domain. In this paper we describe a beam position monitor (b.p.m.) that measures the beam position detecting the resonant field excited by the bunch train in a coaxial cavity. The coaxial cavity is coupled to the beam pipe through four identical slots (see Fig. 1) having the longer side (l) in the beam direction that assure a small coupling impedance of the whole device [1]. The length of the cavity is chosen in order to excite a transverse TE mode. The beam position inside the pipe can be calculated by probing the field in the cavity with a small antenna.

We will describe and compare three different methods to evaluate the signal in the cavity as a function of the beam displacement. The first one is an analytic approach based on the modified Bethe's theory [2]. The second one is based on HFSS [3] simulations and the third one is based on the wire measurements method [4] made on an aluminium prototype.

2 ANALYTICAL APPROACH RESULTS

A sketch of the beam position monitor is shows in Fig.1 with the dimensions of the prototype shown on Table 1.

Considering a bunch train traveling off-axis at a distance r_0 with respect to the center of the beam pipe, the total density current in z=0 can be expressed by the summation:

$$J(t)=\left[\sum_{k=-\infty}^{+\infty} I(t-kT_0)\right]\frac{\delta(r-r_0)}{\pi r_0}\sum_{m=0}^{\infty}\frac{\cos[m(\varphi-\varphi_1)]}{1+\delta_{m0}} \quad (1)$$

where $I(t)$ is the current distribution of the single bunch, T_0 is the bunches spacing and c is the velocity of light. The spectrum of the beam current is:

$$\sum_{k=-\infty}^{+\infty} I(t-kT_0) = I_0 + \sum_{p=1}^{+\infty}\tilde{I}_p\cos(p\omega_0 t) \quad (2)$$

where $\omega_0 = 2\pi/T_0$, I_0 is the average beam current and $\tilde{I}_p$ is the amplitude of the Fourier component at $p\omega_0$ [5]. By assuming a Gaussian bunch distribution we obtain:

$$I(t)=\frac{I_0 T_0 c}{\sqrt{2\pi}\sigma_z}e^{-\frac{1}{2}\left(\frac{z}{\sigma_z}\right)^2} \Rightarrow \tilde{I}_p = 2I_0 e^{-\frac{1}{2}\left(\frac{\sigma_z}{c}\right)^2 p^2\omega_0^2} \quad (3)$$

where σ_z is the rms bunch length.

If a dipole mode of the cavity is tuned in order to resonate at one of the frequencies of the beam power spectrum lines ($\tilde{I}_n$), the average powers extracted by two probes coupled with the two azimuthal polarities (φ_0 and $\varphi_{\pi/2}$) can be expressed as a function of the beam current and transverse displacement in the general form:

$$\begin{cases} P^{(0)} = \underline{P}(\omega_r, r_0, \varphi_1)\tilde{I}_n^2 \\ P^{(\pi/2)} = \underline{P}(\omega_r, r_0, \varphi_1 - \pi/2)\tilde{I}_n^2 \end{cases} \quad (4)$$

Knowing by theory, simulations or calibrating measurements the coefficient $\underline{P}$, the previous system of equations (for a given power spectrum lines $\tilde{I}_n$) allows to calculate, in principle, the values of r_0 and φ_1.

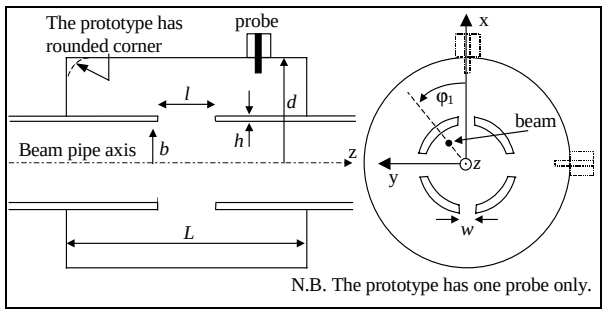

Figure 1: sketch of the beam position monitor.

Table 1: prototype dimensions (mm)

d	30
b	10
L	52
w	2
l	5
h	1

The TE_{111} mode with the polarity φ_0, according to the modified Bethe's theory, dissipates an average power given by [2]:

$$P_{Th.}^{(0)} = \frac{1}{2}\frac{R}{Q}Q_0\cos(\varphi_1)^2 r_0^2\tilde{I}_n^2 \quad (5)$$

where R/Q is given by:

$$\frac{R}{Q}=\frac{4\omega_r\mu A^2\alpha_E^2}{\left(1-2\alpha_E(1+Q)A^2\right)^2+\left(1-2\alpha_E A^2\right)^2} \quad (6)$$

where ω_r and Q_0 are the resonant angular frequencies and the quality factor of the TE_{111} mode, α_E is the electrical polarizability of the single slot and the A coefficient is given by the following integral:

$$A=\frac{\omega_r L\tilde{J}_1(b)}{b\pi c}\left[\int_b^d \frac{L\pi}{2}\left(k_t^2\left(\tilde{J}_1'\right)^2 r+\frac{\left(\tilde{J}_1\right)^2}{r}+\frac{k_t^4L^2}{\pi^2}\left(\tilde{J}_1\right)^2 r\right)dr\right]^{-\frac{1}{2}} \quad (7)$$

with $\tilde{J}_1(r)=J_1(k_t r)-Y_1(k_t r)J_1'(k_t b)/Y_1'(k_t b)$, the prime denote the total derivative with respect to the argument and $k_t=\sqrt{(\omega_r/c)^2-(\pi/L)^2}$.

Considering the prototype dimensions, one obtains the values of ω_r, Q_0 and R/Q reported in Table 2 (first column).

The value of the normalized power $P_{Th.}^{(0)}/Q_0\tilde{I}_n^2$ as a function of r_0 for $\varphi_1=0$ is plotted in Fig. 2 and compared with the simulation and measurement results (described in the next section). In Fig. 3 the same quantity is plotted as a function of φ_1 for r_0=0.6 mm.

Table 2: theory, simulations and measurements results

	THEORY	**HFSS**	**MEAS**
ω_r [GHz]	3.78	3.74	3.74 (tunable)
Q_0	9600	9100	3500
R/Q [mΩ]	36	31	39

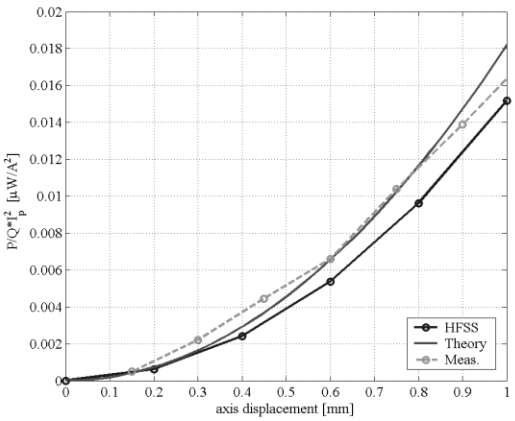

Figure 2: $\underline{P}^{(0)}/Q\tilde{I}_p^2$ as a function of r_0 for φ_0=0.

3 SIMULATION RESULTS

To compare the analytical results with the numerical simulations, we have studied the coupling impedance of the cavity for the TE_{111} mode as a function of the transverse displacement r_0 and φ_1. We have, therefore, calculated the longitudinal shunt impedance of the mode (R_s) for different axial positions, using the Eigenmode Solver of HFSS.

The HFSS model is shown in Fig. 4 with the obtained E field lines. It is only 1/8 of the structure with proper magnetic and electric boundary conditions on the symmetry planes. The average dissipated power in the cavity corresponding to the TE_{111} mode is given by:

$$P_{Sim.}^{(0)}=\frac{1}{2}R_s(\varphi_1,r_0)\tilde{I}_n^2 \quad (8)$$

The value of $P_{Sim.}^{(0)}/Q\tilde{I}_n^2$ is plotted in Figs. 2-3 and compared with the analytical and measurement results. From the previous plot it is possible to verify that it is possible to write the eq. (8) in the form:

$$P_{Sim.}^{(0)}\cong\frac{1}{2}\frac{R}{Q}Q_0\cos(\varphi_1)^2 r_0^2\tilde{I}_n^2 \quad (9)$$

The values of ω_r, Q_0 and R/Q obtained by the simulations are reported in Table 2 (second column).

If the cavity is coupled through a small probe to an external load, then the average dissipated power in the system is still given by eq. (5) or (9) but with Q_0 replaced by the loaded Q_L. The average power dissipated in the load ($P_{Ext}^{(0)}$) is related to the power dissipated in the cavity by:

$$P_{Ext}^{(0)}=P_{cav}^{(0)}\beta/(1+\beta) \quad (10)$$

where β is the coupling coefficients between the probe and the cavity mode TE_{111} and it can be obtained from reflection measurement at the probe port.

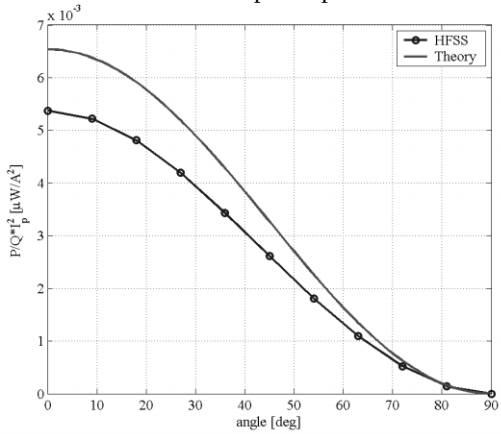

Figure 3: $\underline{P}^{(0)}/Q\tilde{I}_p^2$ as a function of φ_1 for r_0=0.6 mm.

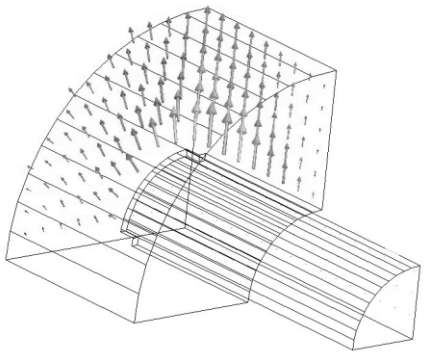

Figure 4: HFSS model with E field lines.

4 PROTOTYPE MEASUREMENTS

Wire measurements have been performed on the aluminum prototype shown on Fig. 5. An antenna probes the signal in the cavity.

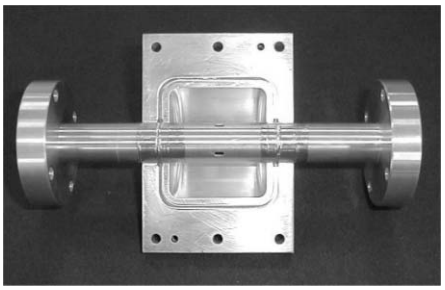

Figure 5: beam position monitor prototype.

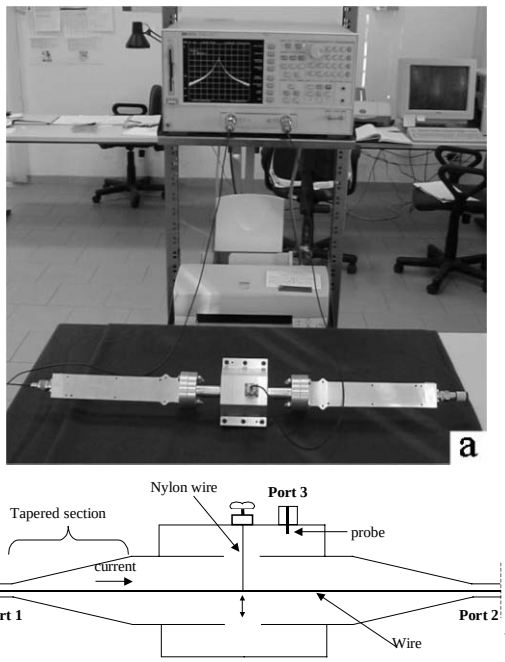

Figure 6: measurement setup

The measurements setup is shown Fig. 6a and schematically represented in Fig 6b. The wire has a radius of 1.5 mm. In order to minimize reflections at the ports 1 and 2 we have inserted two tapered sections that match the 50 Ω impedance of the Network Analyzer with the ~114 Ω impedance of the wire in the beam pipe. To excite the dipolar mode TE_{111} the wire inside the beam pipe has been properly displaced from the axis of the beam pipe. To this purpose, a thin nylon wire has been connected to the wire in order to displace it from the beam pipe axis in a controlled way and to excite the polarity φ_0. The measured transmission coefficient S_{21} and S_{31} are shown in Fig. 7 for a displacement of the wire of ~1.5 mm.

The average dissipated power in the cavity is given by:

$$P_{cav}^{(0)} = P_{Ext.}^{(0)} \frac{(1+\beta)}{\beta} \cong \frac{1}{2} Z_c \frac{|S_{31}(\omega_r)|^2}{|S_{21}(\omega_r)|} \frac{(1+\beta)}{\beta} \tilde{I}_n^2 \qquad (11)$$

The plot of $P_{cav}^{(0)} / Q\tilde{I}_p^2$ as a function of r_0 is reported in Fig. 2. It is clear that $P_{cav}^{(0)}$ can be written in the form (5) or (9) and the equivalent R/Q is reported in Table 2. The Q factor of the resonant mode is lower than the theoretical one because of RF losses in the mechanical contacts. Similar considerations than those developed in [6] can be done from the point of view of the induced errors in the measurement setup.

By the system of equations (4) it is possible to calculate the position of the bunches in the beam pipe when the b.p.m is inserted in the accelerator, by the formulae:

$$\begin{cases} r_0 = \dfrac{\sqrt{P_{Ext.}^{(\pi/2)} / \underline{P} + P_{Ext}^{(0)} / \underline{P}}}{\tilde{I}_n} \\ \varphi_1 = \pm \arctan\left(\sqrt{\dfrac{P_{Ext.}^{(\pi/2)}}{P_{Ext}^{(0)}}} \right) \pm \pi \end{cases} \qquad (12)$$

where the calibration coefficient $\underline{P}$ is given by:

$$\underline{P} = \frac{1}{2} Z_c \frac{|S_{31}(\omega_r)|^2}{|S_{21}(\omega_r)|} \frac{1}{r_0^2} \qquad (13)$$

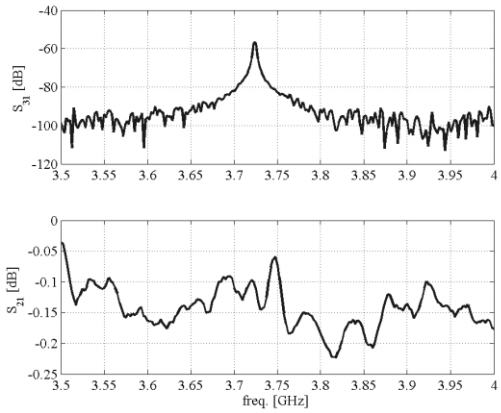

Figure 7: measured transmission coefficients (S_{12}, S_{31}).

5 CONCLUSIONS

A novel bunch position monitor has been described. Measurements on an aluminium prototype have been compared to the theoretical and numerical expectations of the power dissipated by the first dipolar mode in the cavity. The compare shows a good agreement between theory and simulations expecially considering the mechanical differencies between the prototype and the ideal structure. These results confirm the potential application of this device as a beam position monitor. The very low coupling impedance of the device and the possibility of calibration by simple wire measurements make the device hopefully usable in the accelerator machines.

6 REFERENCES

[1] S. De Santis and L. Palumbo, Phy. Rev. E, vol 55, pp. 2052-2055, 1997.

[2] C. D'Alessio, Tesi di Laurea, Univ. "La Sapienza", 2002.

[3] http://www.ansoft.com

[4] F. Caspers, in Handbook of Accelerator physics and engineering, pp. 570-574, World Scientific, 1999.

[5] A. Hofmann, "Beam Instabilities", CERN 95-06, Geneva, 1995.

[6] D. Alesini et al., Proc. of EPAC 2002, pp. 1834-1836, Paris

DESIGN AND STATUS OF THE VISA II EXPERIMENT

G. Andonian*, R. Agustsson, A. Murokh, C. Pellegrini, S. Reiche,
J.B. Rosenzweig, G. Travish, UCLA, Los Angeles, CA 90095, USA
M. Babzien, I. Ben-Zvi, V. Yakimenko, BNL, Upton, NY 11973, USA
L. Palumbo, C. Vicario, Univ. of Rome, "La Sapienza", Italy

Abstract

VISA II is the follow-up project to the successful Visible to Infrared SASE Amplifier (VISA) experiment at the Accelerator Test Facility (ATF) in Brookhaven National Lab (BNL). This paper will report the motivation for and status of the two main experiments associated with the VISA II program. One goal of VISA II is to perform an experimental study of the physics of a chirped beam SASE FEL at the upgraded facilities of the ATF. This requires a linearization of the transport line to preserve energy chirping of the electron beam at injection. The other planned project is a strong bunch compression experiment, where the electron bunch is compressed in the chicane, and the dispersive beamline transport, allowing studies of deep saturation.

INTRODUCTION

The development of a source of high brightness x-rays is an important instrument for studying structural dynamics at the atomic level. The fundamental time scale for atomic motion is on the order of tens of femtoseconds [1]. A single pass self amplified spontaneous emission (SASE) free electron laser (FEL) has the capability to bring about such short pulse x-ray lasers [2]. One way to achieve such high frequency resolution, is to chirp the radiation pulse, then compress the pulse using diffraction gratings. This would reduce the pulse length to the order of tens of femtoseconds [3]. Radiation pulse chirping can be obtained by injecting a chirped electron bunch into the undulator. Theoretical studies have shown that the coherence time is independent of chirp [4], but have yet to be verified experimentally. Another method to drive an x-ray FEL is to inject a short compressed pulse into the undulator.

EXPERIMENTAL OVERVIEW

Summary of VISA I Results

The succesful VISA I experiment was designed to investigate physical properties of SASE-FEL as it relates to future LCLS operation. Saturation was achieved at 840 nm with a SASE power gain length of 17.9 cm and total gain of 10^8. A novel bunch compression mechanism was developed during the VISA I experiment. This scheme utilized second order momentum error effects in the dispersive line. The proper choice of linac phase detuning and quadrupole settings yielded strong longitudinal bunch compression, and as a result, much higher current [5].

Another achievement of the VISA I experiment, was the development and deployment of a start-to-end (cathode to undulator) computational model. The computational effort involved employing UCLA-PARMELA for gun and linac calculations (emittance, charge, energy, energy spread), ELEGANT for transport lattice calculations (bunch length, beam size, emittance growth after dispersive line), and GENESIS 1.3 for undulator studies (gain length, saturation, angular wavelength, and spectra). This computational undertaking, compared with the detailed experimental data, yielded new levels of insight into the dynamics of SASE FEL processes. The same numerical tools will continue to be used for VISA II.

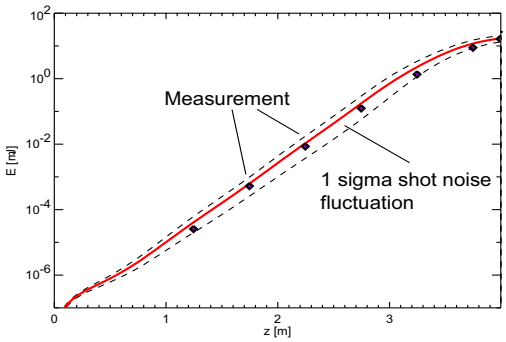

Figure 1: VISA I saturation curve. Measured data is consistent with theoretical calculations.

Experiment Setup

VISA II will encompass a number of hardware changes to investigate the different regimes mentioned above. The undulator and diagnostics will remain unchanged.

Chicane: The chicane compressor consists of four dipole magnets with a nominal field of 0.2 T. The dipoles have a bend radius of 1.2 m and a length of 41 cm. The effective magnetic length is 44.6 cm, with a path length of 41.89 cm. Once the chicane is installed, the electron bunch is expected to compress from 300 μm to less than 30 μm [6]. The current of the bunch is projected to increase from 60 A (VISA I uncompressed running conditions) to 1 kA. Simulations also show that coherent synchrotron radiation

* gerard@physics.ucla.edu

(CSR) may amplify during compression and in the process microbunch the electron beam. Emittance degradation of 4-10 mm mrad is anticipated [7].

The initial experiment to be performed at VISA II is running the FEL with a short compressed beam (current of 1 kA, charge of 200 pC). According to GENESIS 1.3 simulations, the short compressed bunch should produce extremely high gain. Saturation is expected by the 3rd meter of the 4 meter long undulator (Fig.2). With additional compression, the slippage can be so severe that the gain may not be purely exponential.

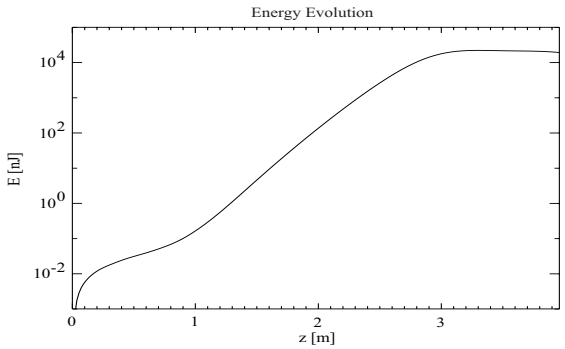

Figure 2: GENESIS 1.3 simulation of the energy evolution within the undulator. Saturation is reached at approximately 3 m, well before the undulator end.

Linearization of Transport: In order to maintain a chirped electron bunch from the linac to the undulator, the transport to beamline 3 must be linearized. Linearization requires a stronger control of the dispersion along the dog leg. The addition of sextupoles will allow VISA II to run in two distinct modes. By diminishing the T_{566}, the linear phase space chirp is maintained, as is illustrated by the ELEGANT simulations in Fig.3. The sextupoles are 5 cm long and have a calculated gradient of 22.0 T/(m^{2}A) [8].

Undulator: The VISA undulator is 4 m long and divided into 4 sections. There are a total of 220, 1.8 cm long periods. The on-axis peak field is about 0.75 T. The undulator has a superimposed quadrupole focusing channel (FODO lattice) throughout the length of the undulator. The electron beam walk-off tolerance inside the undulator is approximately 80 μm [9]. The quadrupoles were aligned so that the beam trajectory would meet this tolerance . Undulator alignment is conducted via a CCD based optical monitoring system [10].

There are eight intra-undulator diagnostics located 50 cm apart. Each port has a double-sided silicon mirror which leases the ability to measure both SASE radiation properties, by reflecting FEL light into the diagnostics, as well as electron beam position and envelope outline, by generating optical transition radiation (OTR) for the beam imaging diagnostics [11].

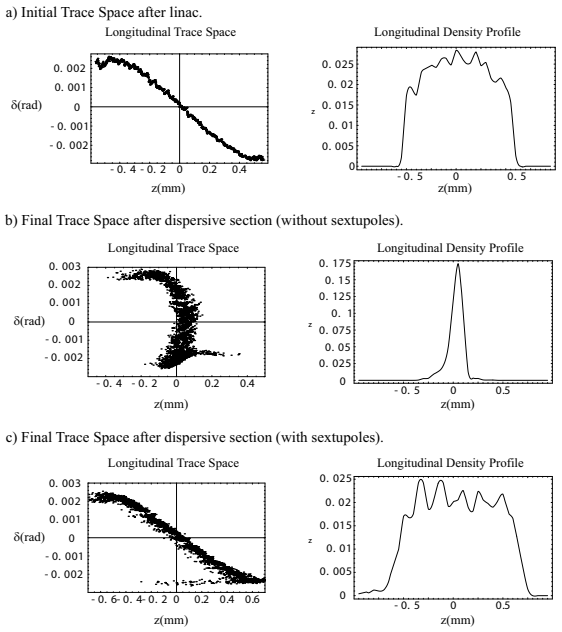

Figure 3: ELEGANT simulations of electron beam linear chirp preservation through dispersive line. VISA II can be run in two distinct modes: the compressed case, due to the natural R_{56} of the dog leg, and the energy chirped case, where the sextupoles are turned on.

CHIRPED PULSE MEASUREMENTS

Conditioning

By accelerating the electron beam at an off-crest RF phase, a linear chirp (energy spread - longitudinal position correlation) may be imparted onto the beam. Once sextupoles are utilized the T_{566} component of the transfer matrix can be minimized, allowing control of the linear chirp throughout the beamline. The input linear chirped phase space will be preserved and injected into the undulator. This will allow control of the frequency distribution of the generated radiation pulse. The natural negative R_{56}, discovered from the original VISA runs, stretches the pulse slightly. However, altered compressor settings can make the R_{56} positive. Experimental and computational analyses will determine various modes of operation, balancing compression, linearity, and degree of chirping. The initial measurement for VISA will be to run with the largest possible chirp obtainable, without degrading the FEL gain. Preliminary calculations show that this chirp is on the order of 4-5 $\%$. In addition, the beam may be partially precompressed in the chicane, without removing its chirp, to raise the current in a chirped beam expertiment.

Simulation Results

Numerical studies have been conducted on the spectral response of a driving initially chirped electron beam. Simulations show that total energy at saturation is not affected

by chirping up to 4 % (no gain degradation), even for the case of the 60A (uncompressed) beam. It is necessary to exceed 2 % chirp to overcome the intrinsic frequency width of the FEL amplification in order to achieve a measureable correlation between frequency and time.

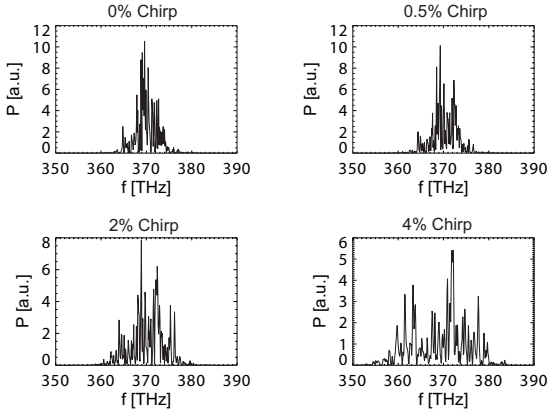

Figure 4: GENESIS 1.3 simulations of chirped pulse radiation spectrum (frequency domain) for varying degrees of chirping.

Proposed Measurements

The goals of the chirped beam experiment are to determine the gain length as a function of degree of chirping, and to measure the spectral correlation of the output beam. Theoretical studies show that the effects of the electron beam chirp on FEL is small if the resonant radiation frequency change within a cooperation length is small [4]. These results must be verified experimentally. FEL properties to be measured include saturation power, intenstiy fluctuations, and spectral and angular properties of the chirped radiation.

The wavelength chirping of SASE radiation can be used to make pulses on the order of 100 fs. Using a monochromator and double diffraction grating the radiated output can be compressed. This encompasses a few experimental complications. Creating short pulses on the order of 10 fs from pulses already on the order of 10 ps, is an experimental challenge. Measuring such short pulses requires reliance on nonlinear effects in materials.

The proposed scheme to measure this output is named Frequency Resolved Optical Grating (FROG) [12]. The signal is split and recombined to overlap at different times in a nonlinear, frequency doubling, crystal. The doubled output light has a time dispersed axis and is sent to a spectrometer which disperses frequency in the other dimension. Standard algortihms are used to reconstruct amplitude and phase informatin of the input radiation. A simplified FROG device (Grenouille), using a thick nonlinear crystal and a Fresnel biprism, yields a simplified single-shot, ultrashort-pulse intensity-and-phase reconstruction device [13]. The measurement of the epxected pulses will be simplified in operation by the use of Grenouille.

EXPERIMENTAL STATUS

The VISA II program is in its initial stage. The Particle Beam Physics Lab (PBPL) of UCLA has developed and is presently installing a chicane compressor for the ATF at BNL. The chicane magnets, vacuum vessel, and coherent synchrotron radiation (CSR) diagnostics have been developed at UCLA. The hardware installation of the chicane is nearing completion. The improvements to the diagnostics on the dispersive line and the mathcing line are underway. The addition of sextupoles will take place in the early summer of 2003, coincident with the chicane dipole installation.

Initial runs for VISA II are dedicated to bringing the beam up to successful operating conditions. The upgraded facilities of the ATF require revising the original run settings; technicalities must be addressed to reestablish high gain lasing conditions. Preparatory runs have yielded successful characterization of beam envelope evolution, and emittance measurements, utilizing the quadrupole scanning technique, are imminent. Optical methods have been used to measure the undulator alignment, however, they have been indeterminate as to whether undulator alignment is adequate. Undulator electron beam trajectory measurements are forthcoming and will be used to confirm alignment before any attempts to re-align are undertaken.

ACKNOWLEDGEMENT

This work is supported by ONR Grant # N00014-02-1-0911.

REFERENCES

[1] G.K. Shenoy, J. Stoehr (eds.), *LCLS - The First Experiments*, Stanford (2000)

[2] C. Schroeder *et al.*, J. Opt. Soc. Am. **B 19 (8)**, 1782-1789 (2002).

[3] C. Pellegrini, Nucl. Inst. & Meth. Phys. Res. **A 445**, 124-127 (2000)

[4] S. Krinsky and Z. Huang, Phys. Rev. STAB **6**, 050702 (2003)

[5] A. Murokh *et al.*, Phys. Rev. **E 67** (2003)

[6] R. Agustsson, M.S. Thesis, UCLA (2003)

[7] R. Agustsson, private communications.

[8] J. England, private communications.

[9] P. Emma and H.D. Nuhn, FEL Proc. 1998, **II**, 35

[10] A. Tremaine, A. Murokh, and X. Wang, BNL Rep. No. 68170 (2001)

[11] A. Murokh, Ph.D. thesis, UCLA, 2002

[12] R. Trebino *et al.*, Rev. Sci. Inst. **68**, 3277-3295 (1997).

[13] P. O'Shea *et al.*, Opt. Lett., **26**, 932-4 (2001).